Bulletin of the Geological Survey of Japan, vol. 64 (1/2), p. 1 - 24, 2013

Article

Zircon and REE-rich alkaline plutonic rocks intruded into the accretionary prism at the Cape Ashizuri, Shikoku Island, Japan

Shunso Ishihara[1, *] and Mihoko Hoshino[2]

Shunso Ishihara and Mihoko Hoshino (2013) Zircon and REE-rich alkaline plutonic rocks intruded into the accretionary prism at the Cape Ashizuri, Shikoku Island, Japan. *Bull. Geol. Surv. Japan*, vol. 64 (1/2), p. 1-24, 14 figures, 7 tables, 3 plates.

Abstract: The Cape Ashizuri body is a small, 12 km^2, Miocene plutonic complex having gabbroids, syenite, quartz syenite to syenogranite in its southern half and biotite monzogranite in its northern half, right next to the Shimanto accretionary sediments. Chemical analyses indicate that the granitoids have mostly meta-aluminous value of A/CNK<1.0, except for three monzogranite. The granitoids are rich in K_2O, plotted in the shoshonite-high K fields. The granitoids are also rich in Na_2O and Rb. Ga content is higher than 18 ppm, indicating characteristics of the A-type granitoids. A distinct characteristic of the Cape Ashizuri granitoids is predominance of HFSE (high-field- strength-element), such as Zr (<1,220 ppm), Hf (25.6 ppm), Nb (<202 ppm), Ta (<14 ppm), LREE (<1002 ppm), HREE (<50.5 ppm), Y (<74 ppm), Th (74.2 ppm). Fluorine is also enriched up to 0.43 wt.%.

These HFSE are contained in such common accessory minerals as zircon, ilmenite, allanite and titanite, and rare minerals of fergusonite, chevkinite and others. Zircon is the most common and visible rarely by naked eyes. Zircon in the highest Zr rock, 58A142 sample, contains the maximum values of 2.4 wt.% HfO_2 and 1.0 wt.% Y_2O_3. Ilmenite in the 58A142 sample shows 4.3-5.7 wt.% MnO, but that in other quartz syenite shows lower values as 1.7-1.8 wt.% MnO, while its niobium content, up to 3.8 wt.% Nb_2O_5, is seen along the rim, indicating the niobium concentrated at the latest magmatic stage. Allanite shows Mn-poor character of the magnetite series (0.44 wt.% MnO), and contains 24.6-25.8 wt.% LREE.

The most mafic phase of the gabbroids is 47.0 wt.% SiO_2 and 12.5 wt.% MgO, indicating its origin of the upper mantle. Quartz syenitic rocks have 55-60 wt.% SiO_2 and low Sr_0 ratio of 0.7035, implying a small degree of the partial melting of mafic igneous source rocks in the lower crust for the alkaline rocks. The high contents of HFSE and F were caused by this small degree of the partial melting. The biotite monzogranite in the northern part is considered as a mixed magma generated from the lower igneous crust and overlying accreted sediments of the Shimanto Supergroup. It is interesting to explore hydrothermal REE concentration related to these plutonic and subvolcanic activities.

Keywords: Cape Ashizuri, Miocene, alkaline granite, zircon, REE

1. Introduction

There are many small Miocene granitic stocks intruded into accreted clastic sediments of the late Paleozoic to Tertiary age in the western Shikoku and eastern Kyushu districts in Japan (Fig. 1). These stocks belong generally to calc-alkaline I-type ilmenite-series and are not particularly high in the rare earth elements (REE: Cullers and Graf, 1984), except for one locality at the Cape Ashizuri, southwestern edge of the Shikoku Island. This body contains both alkaline and calc-alkaline plutonic rocks, the alkaline rocks of which were considered to be formed by alkaline metasomatism of the late magmatic stage (Murakami and Matsuo, 1963), but later re-interpreted that they are intrinsically alkaline magma (Murakami and Masuda, 1984; Murakami and Imaoka, 1985) rich in fluorine with relatively low water and low to moderate oxygen fugacities (Murakami *et al.*, 1983).

The Cape Ashizuri granitoids are considered to belong to A-type for the high Ga contents (Imaoka *et al.*, 1991). Besides the alkalinity, this pluton is different from the others in the Outer Zone of Southwest Japan (e.g., Okueyama pluton) having a moderate contents of rock-forming magnetite (Ishihara, 1979) and a low initial $^{87}Sr/^{86}Sr$ ratio (Sr_0) of 0.7035 (Shibata and Ishi-

[1]AIST, Geological Survey of Japan

[2]AIST, Geological Survey of Japan, Institute for Geo-Resources and Environment

*Corresponding author: S. ISHIHARA, Central 7, 1-1-1 Higashi, Tsukuba, Ibaraki 305-8567, Japan. Email: s-ishihara@aist.go.jp

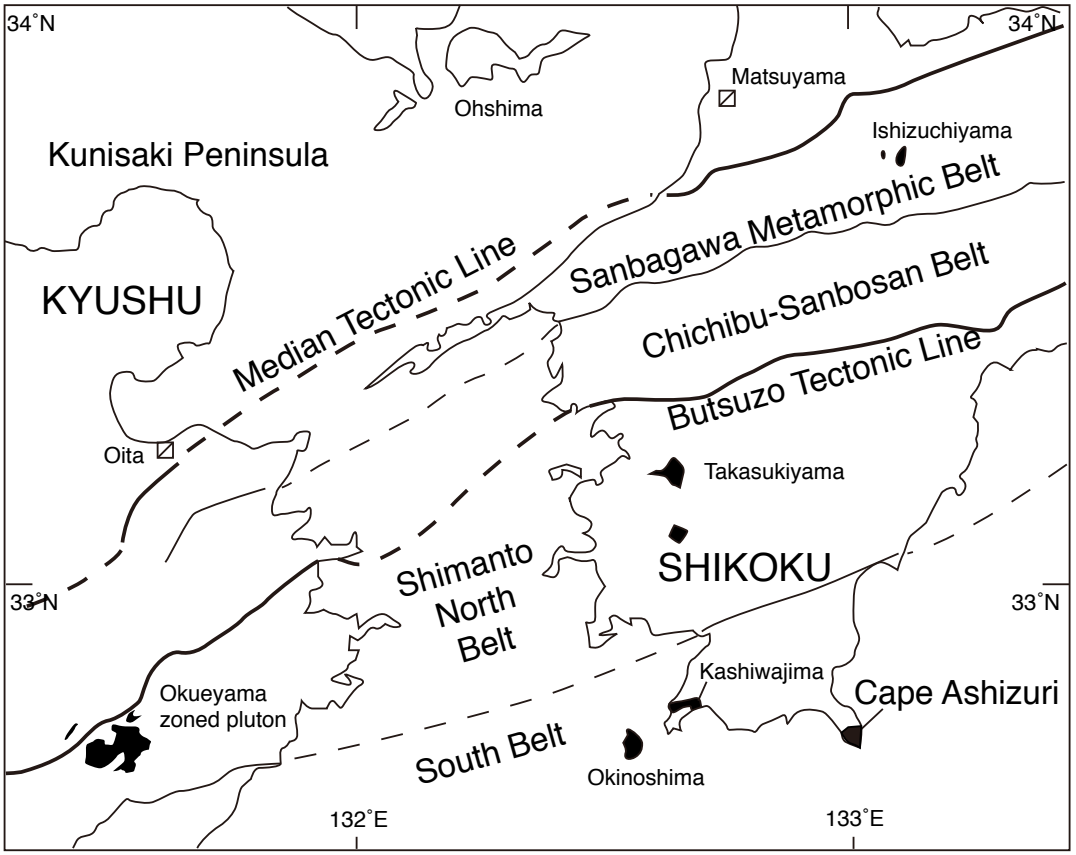

Fig. 1 Accretionary terranes and major faults in the Outer Zone of Shikoku and Kyushu islands from Teraoka *et al*. (1999). Solid mark implying Miocene granitic plutons.

hara, 1979). Zircon can be visible by naked eyes in this pluton, and the zirconium content is the highest at 66 wt.% SiO_2; thus belonging to the high temperature-type granite of Chappell *et al*. (2004). The Cape Ashizuri pluton is, therefore, unique anorogenic granite, occurring in an orogenic environment.

Magnetite and ilmenite were collected from the weathered soil of gabbroic rocks in flat area of the pluton at the north of the community Isa (Fig. 2), and tried to use for coin production in the 18th century by the old Tosa local government. According to re-examination of soil from the gabbroic area after the Second World War, the oxide contents in the soil were measured to vary from 1.33 to 4.12 wt.% (Shibano, 1958), and the oxides sands were considered as Ti-resource. High radioactivity was discovered during uranium exploration stage of 1960s from the abandoned oxides sand. This radioactive sand was composed of ilmenite 67 wt.%, magnetite 15 wt.%, quartz 14 wt.%, zircon 1.7 wt.%, and uranothorite and other heavy minerals 2.3 wt.% (Hayashi *et al.*, 1969).

Ilmenite and magnetite should be contained abundantly in mafic gabbroic rocks remaining as xenolithic bodies, but uranothorite may well be derived from granitic matrix. In order to identify the mode of occurrence of these U-bearing heavy minerals, a shallow drilling was performed in quartz syenite hosting gabbroids near the site of the old mining site in the early 1969 under the then-current uranium project. No gabbroids but only quartz syenitic rocks, together with several sheared zones, were discovered for the depth of 250 meters of the drill hole. The syenitic rocks were high in the radioactivity but no anomalous values were observed on the sheared zone. No evidence of hydrothermal alteration was observed through the drill hole. Potentiality of the rare earth elements was also tested in the weathered crust of the Ashizuri plutonic body, and the results were reported in a separate paper (Murakami and Ishihara, 2006).

Including all the chemical data we have, this paper describes chemical characteristics of the unique granitoids of the Cape Ashizuri pluton intruding into the Shimanto accretionary complex, which was formed under a typical orogenic environment. The data are compared with the I-type ilmenite-series chemistry of the Okueyama pluton (Ishihara and Chappell, 2010), which is vertically zoned calc-alkaline pluton (Takahashi, 1986), occurring in the same Outer Zone of Southwest Japan.

2. Geologic background

Several accreted sedimentary and metamorphic zones

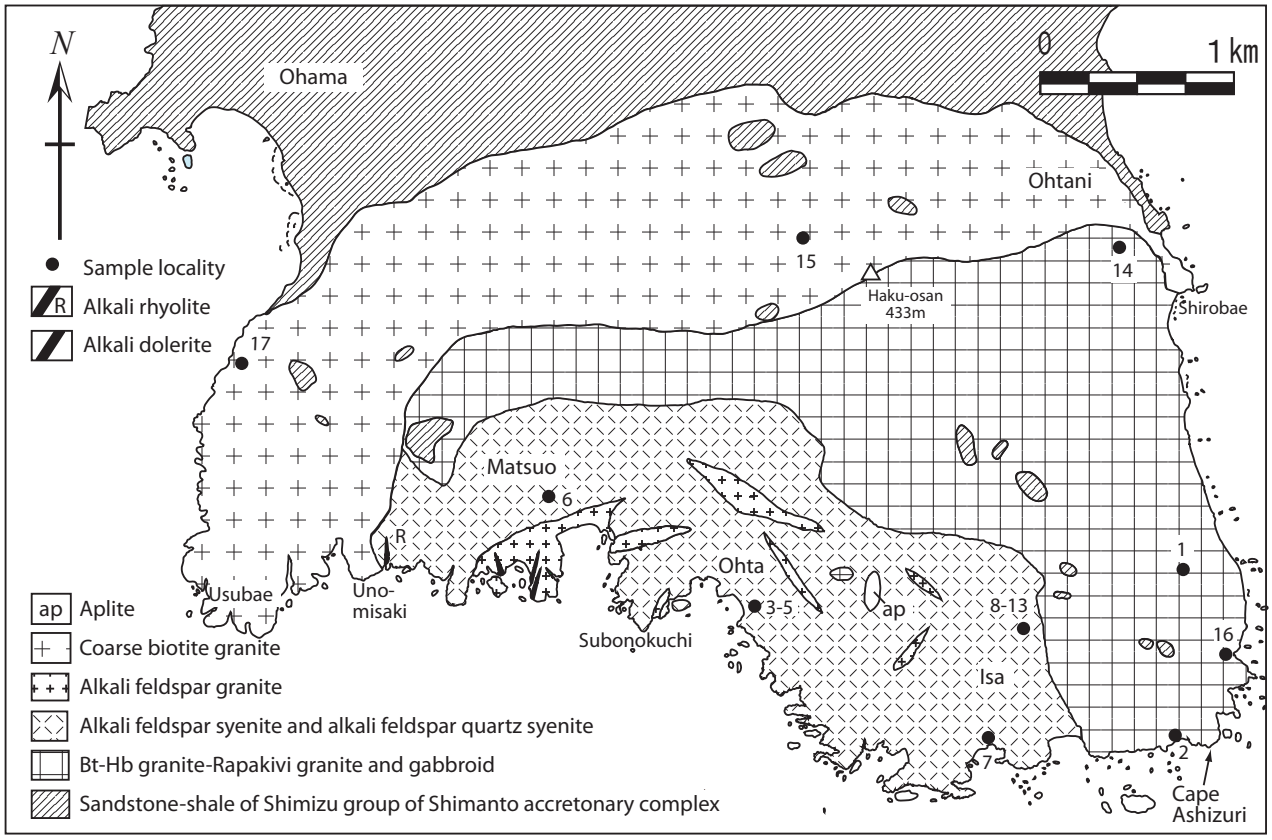

Fig. 2 Rock unit map (modified from T. Imaoka, 1993 unpublished) and location of the analyzed samples. Solid circle with the filing numbers listed in Table 1.

from late Paleozoic to Miocene in age being generally younger toward the southeastern coast with the Pacific Ocean, have been recognized in the western Shikoku Island (Fig. 1). These zones are, from north to south, Sanbagawa metamorphic belt, Chichibu-Sanbosan sedimentary belt and Shimanto sedimentary belt (Fig.1). Accreted sediments of the Shimanto belt are subdivided into the Cretaceous North Belt and Paleogene (-Miocene) South Belt (Fig. 1). The southernmost unit where the Cape Ashizuri intruded is mostly composed of shale having around N75°E strike and steep dip (60-80°) to north (Suzuki, 1938).

The Cape Ashizuri pluton, which is the best observable along the southern coast of the peninsula region (Plate IA), intrudes into the youngest Paleocene-Miocene Shimizu Formation of the Shimanto Supergroup, consisting of the clastics brought from the north (Teraoka, 1979). These clastic rocks were studied chemically, and found that the shales are extremely higher in SiO_2 and lower in Al_2O_3 than older shales occurring to the north, indicating a high maturity of the Paleocene-Miocene shale relative to Cretaceous one (Ishihara *et al.*, 1985). Some of these rocks occur as roof-pendant and xenolithic fragments in the biotite monzogranite phase of the Cape Ashizuri pluton (Fig. 2).

The pluton has an exposed area of 12 km^2 on land, and is composed of three intrusive units as, (1) syenite-alkaline granites along the south coast, (2) gabbro and syenite/granites mingled phase, occurring the middle part (gabbro less than 25 vol.%) and (3) biotite monzogranite. The intrusive sequence appears to be the gabbroids, syenites, and then monzogranite. The second unit gabbroids are essentially pyroxene gabbro, but are often converted to dioritic rocks by the mingling and interaction with syenitic rocks. Thus, they are closely associated genetically each other. The monzogranite is a normal monzogranite occurring everywhere in the Japanese orogenic belts. Several alkaline (4.53 wt.% K_2O) dolerite dikes and a few peralkaline rhyolite dikes, very rich in rare earth elements (Ishihara *et al.*, 1990), cut in N-S direction of the western part of the unit 2.

About the radiometric age of the Cape Ashizuri body, Shibata and Nozawa (1982) summarized K-Ar ages on one hornblende and two biotites to be 13 Ma. Iizumi and Murakami (1980) obtained Sr isochron age of 15.6±2.1 Ma for the stage II syenite and alkali granite, and 11.5±0.5 Ma for the Stage IV granites. Murakami *et al.* (1989) added K-Ar ages of two whole rocks of 12.0±0.6 and 14.0±0.7 Ma and one biotite age of 12.9±0.6 Ma, and five fission track ages varying widely from 10.0±1.8 to 16.1±0.7 Ma.

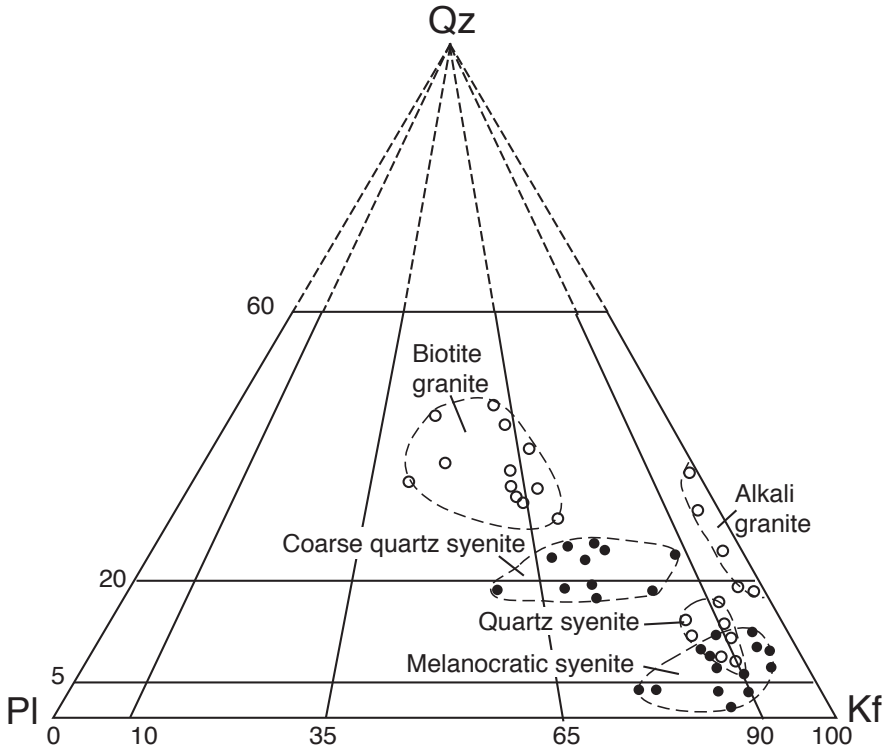

Fig. 3 Modal composition of various granitic rocks of the Cape Ashizuri pluton.

Recent U-Pb ages on zircons must be more reliable than the K-Ar ages, They are 13.12±0.09 Ma for syenite along south coast and 12.95±0.06 Ma for monzogranite at north (Shinjoe *et al.*, 2010). Gabbroids are mingled with these syenite and granite. Thus, all the plutonic rocks intruded in a short period around 13 Ma, but alkali dolerite and alkali rhyolite dike may be younger, because they intruded after solidification of the plutonic body. This Miocene intrusion age is very close to the youngest age of sedimentary rocks of the southernmost Shimanto Supergroup.

Modally speaking, the granitoids are plotted from K-feldspar corner to syenogranite and monzogranite areas (Fig. 3; Murakami and Matsuo, 1963; Hayashi *et al.*, 1969). Mapping this pluton in 1993, Imaoka and his student (personal communication, 2011) recognized three plutonic units:(1) Gabbroids mingled with Rapakivi granite and biotite-hornblende granite, which are typically shown at the Cape Ashizuri (see Plate 1B), (2) Alkaline granite unit occurring along the south coast, which is composed of various grain size of syenite and quartz syenite, and locally alkali feldspar granite, (3) Coarse-grained monzogranite intruded into the above two units (Fig. 2). As mentioned previously, the units 2 and 3 are intruded at 13.12 and 12.95 Ma, respectively, on U-Pb zircon age.

Murakami *et al*. (1989) proposed a ring complex model for the formation of these rocks, having different source rocks with low initial $^{87}Sr/^{86}Sr$ ratio of 0.7038 for the inner gabbroic and syenitic rocks (Unit 1), and higher 0.7059 value for the outer granite (Unit 3). Therefore, the quartz-free plutonic rocks have a deeper, more primitive source rocks than the quartz-bearing rocks of continental crust, which is supposed to be the youngest members of the Shimanto Supergroup.

3. Chemical characteristics

Chemical analyses of the gabbroic and granitic rocks were newly performed on 17 samples by the Code 4E-research set of the Actlabs, which is done by the total digestion – ICP/MS and lithium metaborate fusion – ICP/MS for 50 major and trace elements, but S by infrared and F by ISE (see the Actlabs webpage for the details: http://www.actlabs.com/). The detection limits and analytical results are listed in Table 1.

In the syenitic rocks, well digested mafic enclaves are sometimes observed. Two examples (Nos. 3 and 4, Fig. 2) of the 58A124 site are high in mafic components such as TiO_2 (1.4-1.6 wt.%), total Fe_2O_3 (8.9-9.1 wt.%), MgO (2.5-2.8 wt.%) and Zn (235-258 ppm) for the SiO_2 55.2-55.5 wt.% rocks. These granitoids may contain zincian ilmenites described by Nakashima and Imaoka (1998) for the high bulk Zn contents (Table 1). Another feature is general high contents of fluorine in the Cape Ashizuri granitoids, especially in the 58A124 rocks of 0.43-0.26 wt.% F. Zirconium contents are also high in the Cape Ashizuri granitoids, in which the highest of 1,220 ppm is seen in the 58A142 quartz syenite.

A drilling for uranium exploration was performed in winter of 1969 at the northern-off part of the community Isa (Fig. 2), southwest of the old placer mining site.

Table 1 Chemical composition of the Cape Ashizuri plutonic rocks.

Filing No.		1	2	3	4	5	6	7	8	9	10	11	12	13	14	15	16	17
Anal. Sym.	Det.Lmt.	58A102	58A101	58A124	58A124M	58A124F	58A126	58A142	DH38.0	DH66.9	DH96.3	DH145.2	DH180.1	DH210.6	58A118	69AZ01	58A152	58A130
SiO2	0.01	51.39	63.62	55.23	55.51	70.59	55.6	66.26	67.1	65.69	64.99	66.09	67.85	66.49	70.08	72.77	73.1	76.08
TiO2	0.001	1.374	0.912	1.382	1.613	0.22	1.915	0.317	0.32	0.357	0.31	0.394	0.351	0.367	0.383	0.371	0.165	0.204
Al2O3	0.01	14.51	14.6	15.25	15.95	13.95	15.39	15.43	15.62	15.95	15.6	16.06	15.31	16.04	13.97	13.46	13.13	12.18
Fe2O3(T)	0.01	8.79	5.6	9.06	8.9	2.16	9.79	3.74	3.93	4.15	3.12	3.77	3.22	3.33	2.55	2.6	2.26	1.7
MnO	0.001	0.146	0.102	0.186	0.184	0.062	0.2	0.103	0.095	0.129	0.073	0.076	0.065	0.074	0.042	0.044	0.024	0.025
MgO	0.01	6.91	2.42	2.45	2.84	0.07	3.25	0.12	0.14	0.18	0.2	0.32	0.29	0.34	0.56	0.44	0.08	0.21
CaO	0.01	11.4	4.69	3.88	4.65	0.83	6.48	0.93	1.04	1.39	1.1	1.16	0.91	1.14	1.16	1.21	0.32	0.65
Na2O	0.01	2.46	3.87	5.73	5.89	4.74	4.22	5.1	5.1	5.26	4.97	5	4.55	4.78	3.25	3.53	3.58	3.28
K2O	0.01	1.56	3.79	3.34	3.02	5.11	2.51	5.49	6.26	5.77	6.34	6.28	6.17	6.3	5.98	4.82	6.76	4.52
P2O5	0.01	0.28	0.21	0.47	0.56	0.03	0.52	0.03	0.04	0.05	0.04	0.07	0.06	0.07	0.09	0.09	0.04	0.04
LOI		1.15	0.57	1.17	0.78	0.6	0.65	0.48	0.3	0.46	0.38	0.34	0.41	0.39	0.55	0.46	0.2	0.36
F	0.01	0.07	0.14	0.34	0.43	0.26	0.17	0.1	0.11	0.17	0.12	0.13	0.13	0.12	0.1	0.13	0.02	0.1
S	0.001	0.107	0.044	0.01	0.02	0.003	0.017	0.02	0.006	0.006	0.004	0.004	0.003	0.002	0.005	0.011	0.002	0.008
Total	0.01	99.98	100.4	98.16	99.89	98.36	100.5	98	99.95	99.38	97.13	99.56	99.19	99.33	98.61	99.81	99.65	99.24
Rb	1	48	133	311	284	281	126	251	239	257	229	250	214	228	239	229	346	284
Cs	0.1	0.9	2.1	7.3	5.4	4.4	2.5	2.6	5.5	3.6	6.8	4.8	6	4.9	6.3	34.4	2.8	9.4
Sr	2	405	203	247	346	19	298	12	13	17	30	47	49	68	84	71	24	31
Ba	1	1189	586	1607	1755	199	623	101	126	158	223	354	393	575	679	411	169	171
Ga	1	15	20	20	21	26	22	26	24	24	23	25	22	24	19	20	24	19
Ge	0.5	1.8	2.2	1.8	2	2	2.1	2.3	2.5	2	2.1	2.6	2.2	1.7	1.9	2	2.1	2
Zr	1	131	186	216	241	487	203	1220	684	799	739	706	606	581	275	275	386	235
Hf	0.1	3.1	4.7	5.5	5.9	12.1	5.3	25.6	13.7	16.8	17.2	16.2	13.8	13.3	7.1	7.7	9.9	7.4
Nb	0.2	38.3	80.5	91.2	110	162	79.7	202	141	173	144	151	118	118	47.4	59.4	122	40.4
Ta	0.01	2.68	6.13	8.04	7.57	11.1	6.87	14	9.45	11.3	10.6	9.2	7.85	7.37	3.62	6.01	10.9	5.98
Be	1	1	3	5	5	4	4	5	4	6	4	4	3	3	3	4	6	5
Sn	1	1	13	15	12	5	7	5	6	5	4	6	5	4	4	5	4	4
W	1	20	50	21	15	31	24	49	13	20	21	15	19	21	87	84	54	78
Mo	2	< 2	< 2	< 2	< 2	< 2	< 2	< 2	< 2	2	11	< 2	< 2	< 2	< 2	5	< 2	< 2
Th	0.05	9.04	25.4	23.6	14.9	51.5	14.5	74.2	36.5	66.3	63.3	50.8	56.2	37.4	24.2	43.5	53.2	69.1
U	0.01	1.63	4.1	5.56	3.65	9.86	3.33	8.6	6.91	12	7.03	5.7	8.27	6.59	3.47	8.27	11.4	11.3
Cr	0.5	32.3	17	17.6	14.4	< 0.5	< 0.5	3.6	< 0.5	< 0.5	< 0.5	< 0.5	< 0.5	< 0.5	8.4	5	< 0.5	3.8
V	5	285	130	115	120	< 5	249	< 5	< 5	< 5	9	12	10	9	32	21	6	10
Co	0.1	39.9	26	15.5	17.4	5	29	9.7	2.4	4.4	4.9	4.2	5	5.3	16.4	15.7	10.9	13.9
Ni	1	52	23	16	17	2	12	2	2	1	2	2	1	2	4	5	2	3
Cu	1	116	36	3	4	3	19	4	3	4	1	5	< 1	2	3	< 1	1	2
Zn	1	55	60	235	258	68	126	75	78	78	59	64	55	56	40	42	28	30
Pb	5	< 5	< 5	5	15	12	8	< 5	10	7	6	< 5	9	6	10	7	< 5	< 5
As	1	2	1	5	2	3	2	2	3	3	4	< 1	1	2	3	6	< 1	2
La	0.05	31.8	49.3	65.8	77.2	130	59.8	263	147	118	232	304	98.7	93.4	69.6	75.7	89.8	72.6
Ce	0.05	56.8	103	123	143	224	117	442	257	212	384	498	175	170	125	140	160	132
Pr	0.01	6.33	11.2	13.3	15.4	21.4	12.8	42	24.3	21.7	35.5	44.7	17.2	17.4	12.5	14.2	15.6	12.9
Nd	0.05	24.1	40.3	48.6	56.6	67.5	46.5	132	79	74.7	109	136	57.1	60	42.6	48	49.9	40.7
Sm	0.01	4.8	7.72	9.39	10.7	11.5	8.84	18.6	12.5	13.7	14.8	18.7	10.1	11	7.77	8.96	9.37	6.49
Eu	0.005	1.43	1.17	2.64	3.07	0.543	1.8	0.507	0.641	0.662	0.68	0.914	0.852	1.11	0.875	0.767	0.439	0.355
LREE		125.26	212.69	262.73	305.97	454.943	246.74	898.107	520.441	440.762	775.98	1002.31	358.952	352.91	258.345	287.627	325.109	265.045
Gd	0.01	4.41	6.66	8.33	9.52	9.13	7.39	12.3	9.58	11.2	9.84	13.1	8.44	9.13	6.15	7.44	7.92	4.82
Tb	0.01	0.73	1.13	1.48	1.63	1.64	1.26	2.06	1.56	1.98	1.41	2.03	1.45	1.58	1.08	1.36	1.58	0.88
Dy	0.01	4.22	6.73	8.71	9.64	9.91	7.3	12.2	9.15	11.6	7.94	11.2	8.82	9.3	6.29	8.04	10.1	5.41
Ho	0.01	0.86	1.43	1.88	2.02	2.17	1.52	2.64	1.93	2.42	1.65	2.27	1.89	1.94	1.28	1.67	2.17	1.19
Er	0.01	2.35	4.13	5.38	5.74	6.23	4.29	8.17	5.69	6.99	5	6.46	5.55	5.57	3.53	4.81	6.44	3.64
Tm	0.005	0.361	0.698	0.91	0.935	1.09	0.707	1.47	0.99	1.25	0.894	1.07	0.947	0.954	0.564	0.831	1.16	0.668
Yb	0.01	2.28	4.45	5.53	5.79	6.41	4.34	10	6.41	7.87	5.89	6.66	5.92	5.87	3.45	5.01	6.92	4.32
Lu	0.002	0.318	0.624	0.777	0.818	0.91	0.636	1.65	0.989	1.18	0.934	1.01	0.875	0.858	0.477	0.728	0.95	0.646
HREE		15.529	25.852	32.997	36.093	37.49	27.443	50.49	36.299	44.49	33.558	43.8	33.892	35.202	22.821	29.889	37.24	21.574
Y	1	23	39	61	60	65	41	74	55	67	47	61	52	52	34	45	62	33
Sc	0.01	38.8	15.7	13.5	15.6	1.67	20.8	4	3.94	4.24	3.28	4.74	3.63	4.45	6.34	5.94	1.14	3.17
NK/A		0.40	0.72	0.86	0.81	0.96	0.63	0.93	0.97	0.93	0.96	0.94	0.93	0.92	0.85	0.82	1.01	0.84
Ga10000/Al		1.95	2.59	2.48	2.49	3.52	2.70	3.19	2.90	2.84	2.79	2.94	2.72	2.83	2.57	2.81	3.46	2.95
ASI		0.55	0.77	0.76	0.74	0.94	0.72	0.96	0.92	0.92	0.92	0.94	0.97	0.96	1.00	1.02	0.95	1.06
ZrT°C		636	748	746	748	877	730	975	900	914	906	905	898	888	830	835	859	829

It cuts through fine to medium grained quartz syenitic rocks, which had been sheared in some places. The fresh quartz syenites are relatively high in F, 1,100-1,700 ppm; Zr, 581-799 ppm, and LREE, 353-1,002 ppm, and radioactive components of Th, 37-66 ppm and U, 6-12 ppm. The highest Zr (1,220 ppm) and thorium (74

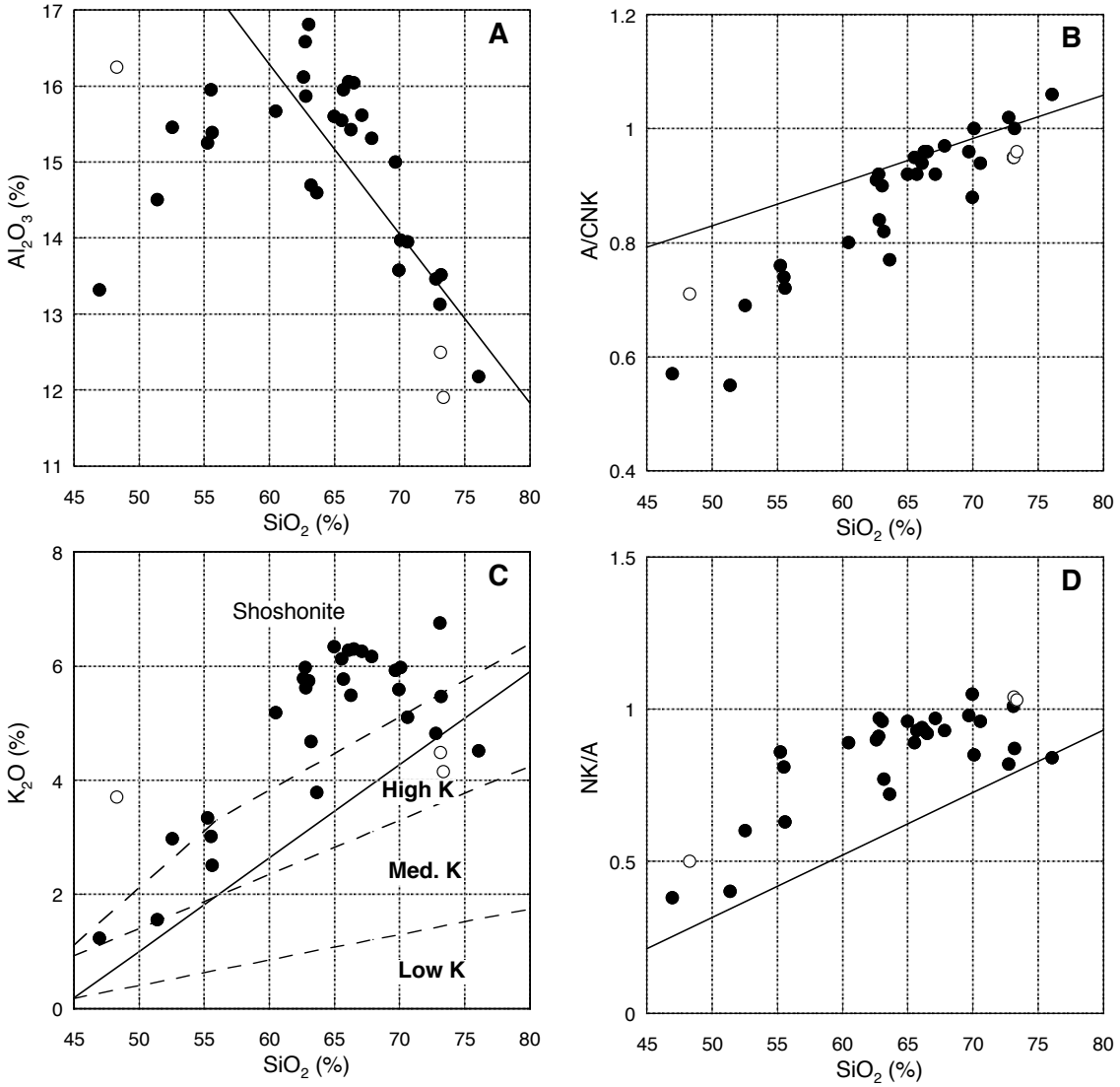

Fig. 4 Harker diagrams for Al_2O_3, A/CNK, K_2O and NK/A. Straight line is an averaged trend of the Okueyama granitoids of Ishihara and Chappell (2010). Open circle, post-plutonic dikes of dolerite (AZ04) and rhyolite (AZ02, 03) from Ishihara *et al*. (1990) for Figs. 4 through 12.

ppm) contents were found at the 58A142 site (No. 6 in Fig. 2).

Chemical data reported in the previous paper (Ishihara and Murakami, 2006) and newly analyzed data in Table 1 are plotted by solid circle in the Harker diagrams from Figures 3 to 7, together with post-plutonic dikes (open circle) of dolerite and rhyolite of Ishihara *et al.* (1990). The straight line in the figures is an average trend of the vertically zoned, Okueyama pluton (Ishihara and Chappell, 2010), which belongs to typical I-type calc-alkaline ilmenite series.

3.1 Harker diagrams

Distribution of Al_2O_3 contents is parallel to that of the Okueyama pluton in the granitic composition (e.g., SiO_2 higher than 65 wt.%), but some gabbroids including diorites, i.e., silica lower than 56 wt.% (e.g., 58A102, 58A124 and 58A126 in Table 1 of this paper; AZR1 and 58A153 in Table 1 of Ishihara and Murakami, 2006), are low in the content of Al_2O_3 (Fig. 4A). Thus, the Cape Ashizuri pluton is clearly separated into gabbroids and granitoids in the alumina-silica diagram. Both dolerite and rhyolite dikes are lower in the Al_2O_3 contents than the plutonic rocks.

In the A/CNK-SiO_2 diagram (Fig. 4B), however, the Cape Ashizuri rocks, both plutonic and dike rocks, are plotted in similar distribution trend decreasing the Al_2O_3 contents sharply to the low SiO_2 side. This would indicate that feldspars of the Cape Ashizuri pluton belong to the same fractionation trend from the gabbroids to the biotite monzogranite. Also peraluminousness increases sharply toward the high silica rocks but never exceeds 1.2. Compared with the Okueyama granitoids, the Cape Ashizuri rocks are lower in the A/CNK ratio; thus less aluminous.

K_2O contents are plotted in the shoshonite and high

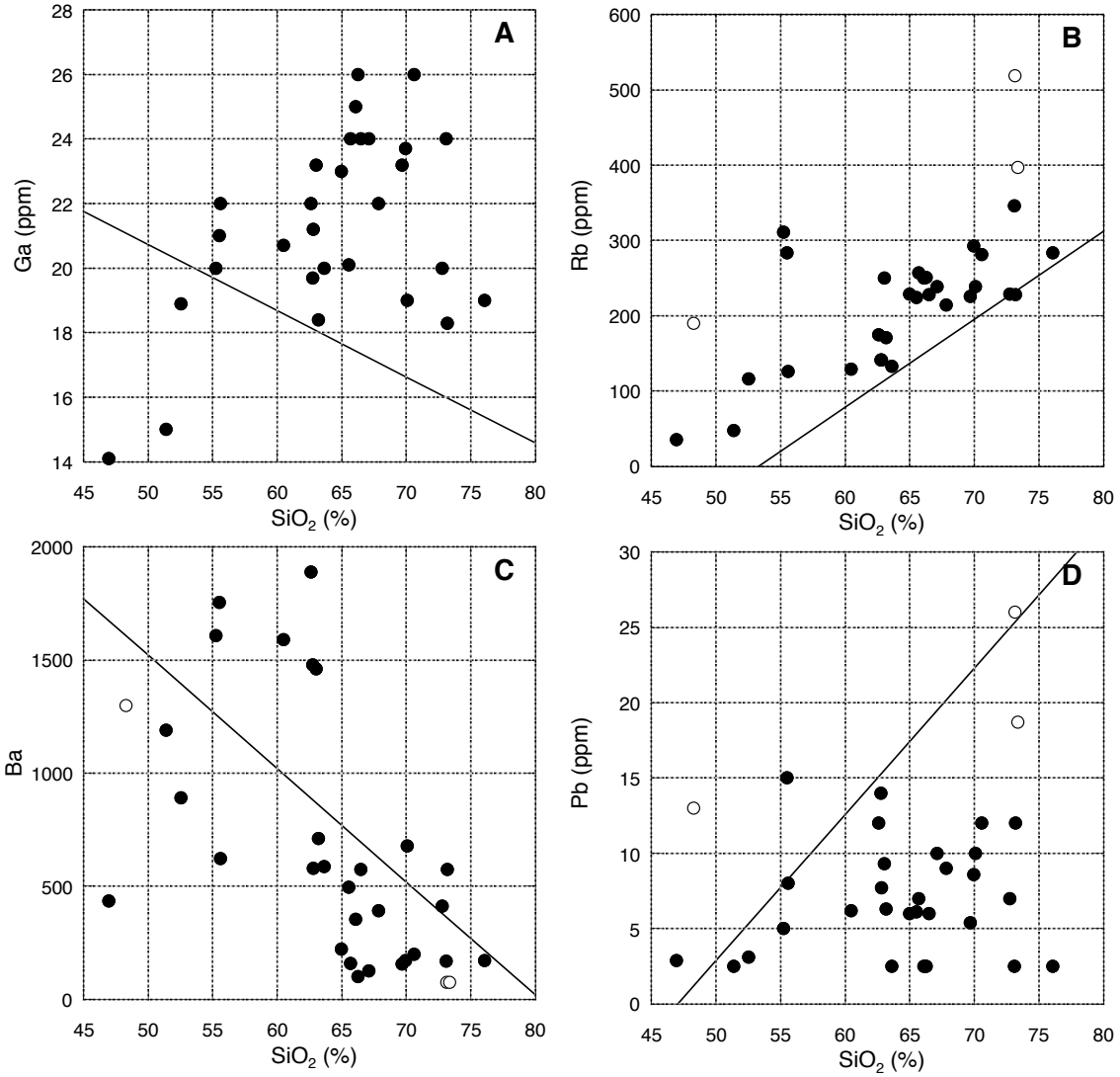

Fig. 5 Harker diagrams for Ga, Rb, Ba and Pb.

K-series areas (Fig. 4C) and are higher than those of the Okueyama granitoids. Three biotite monzogranites and two gabbroids are as low as the Okueyama trend. Dolerite dike is plotted in the shoshonite field, but the two rhyolite dikes are less potassic, plotted in the high-K field. Molecular ratio of sodium and potassium against alumina (NK/A) is constantly much higher than that of the Okueyama pluton (Fig. 4D).

Trace elements which replace Al_2O_3 in feldspars show unusual trend. Gallium (Ga^{3+}, 0.62Å, Mason, 1966), for example, does not follow the amount of Al_2O_3 (Al^{3+}, 0.50Å) and is much higher in felsic rocks than mafic rocks, which is completely different from common distribution trend of calc-alkaline rocks that follow Al_2O_3 contents as seen in the Okueyama pluton. Except for two gabbroids, the Ga contents range from 18 to 26 ppm (Fig. 5A), which are much higher than those of the Okueyama granitoids. This relative abundance was used to define the granitoids as A type by Imaoka and Nakashima (1994), although the geologic environment is not anorogenic but orogenic.

Rubidium (Rb^+, 1.47Å) which replaces K^+ (1.33Å) in K-feldspar shows the same distribution trend as that of the Okueyama granitoids, but the contents are higher (Fig. 5B). Barium (Ba^{2+}, 1.34Å) contents are similar to those of the Okueyama granitoids, decreasing in the content with increasing SiO_2 in general (Fig. 5C). However, the contents are much lower in the rocks with 47-55 wt.% and 63-73 wt.% SiO_2 ranges, but higher in the rocks with 55-63 wt.% SiO_2 range, as compared with the average trend of the Okueyama pluton. Trace amounts of lead (Pb^{2+}, 1.20Å) that takes K-position in K-feldspar, are much lower than those of the Okueyama pluton (Fig. 5D), which ranges from 14 to 40 ppm Pb in the common granodioritic phase and 40 to 70 ppm Pb in the uppermost leucocratic phase (see Ishihara and Chappell, 2010).

CaO contents are generally lower than the average of the Okueyama pluton in the main syenitic rocks (Fig. 6A). On the contrary, Na_2O contents are much higher

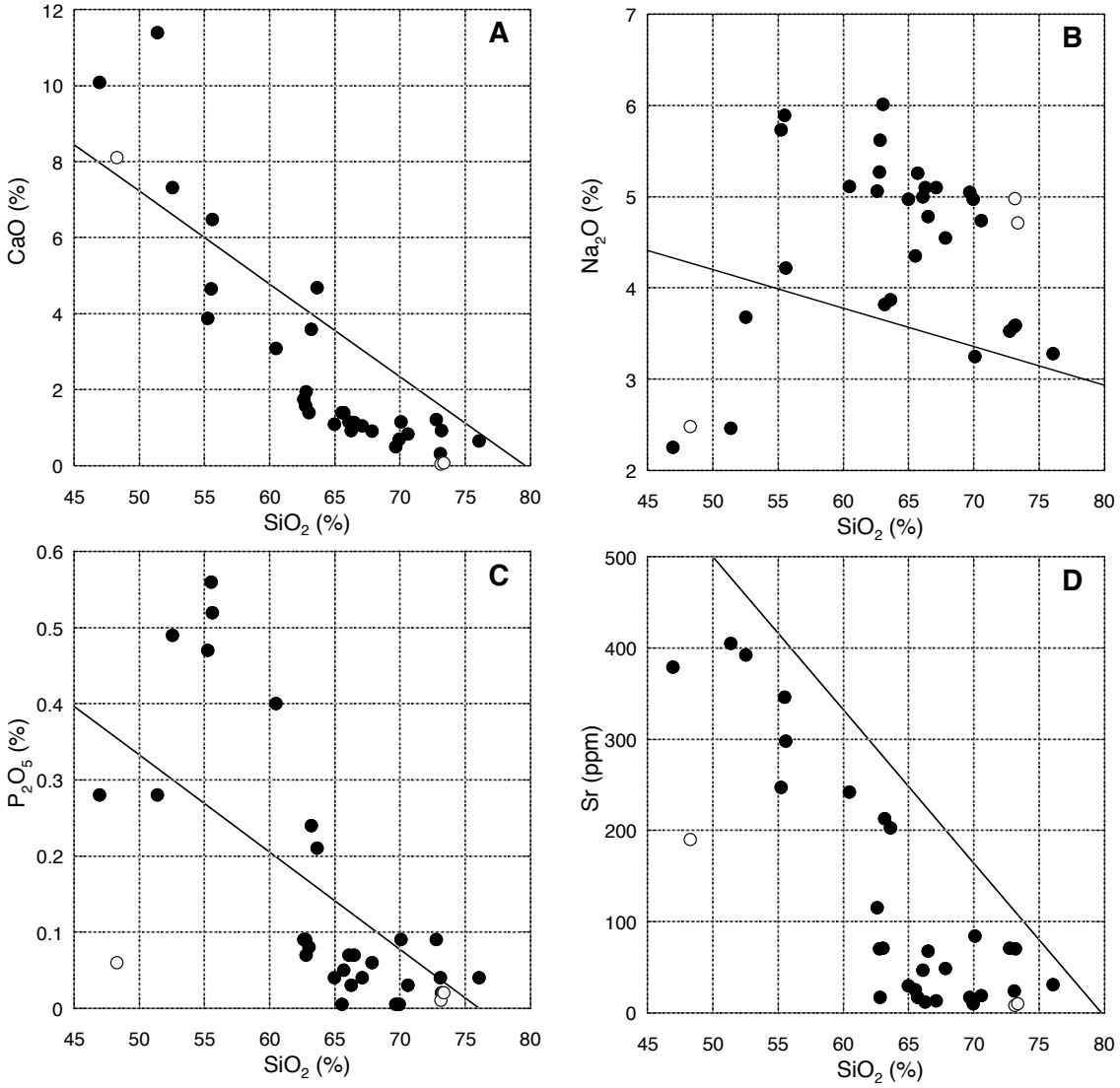

Fig. 6 Harker diagrams for CaO, Na_2O, P_2O_5 and Sr.

than the average contents especially on the SiO_2 55-70 wt.% rocks (Fig. 6B). Two gabbroids high in CaO content are very low in Na_2O content. Thus, these two rocks (58A102 and AZR1) must contain very calcic plagioclase. P_2O_5 contents are very high at around SiO_2 55%, but most of syenitic rocks are lower than the average content of the Okueyama pluton (Fig. 6C). About strontium (Sr^{2+}, 1.12Å), it follows CaO content implying its occurrence in plagioclase (Ca^{2+}, 0.99Å); but the contents are very low in the granodiorite-granite phase (SiO_2 63-76 wt.%). Distribution of Sr is always lower than that of the average value of the Okueyama body (Fig. 6D).

Total Fe_2O_3 contents are slightly lower than the average content of the Okueyama granitoids, but MnO contents are very similar or slightly higher than the average contents of the Okueyama pluton (Figs. 7A, B). Two dikes have similar distribution. Both MgO and TiO_2 contents are different having higher values at low silica side than the Okueyama average, but depleted in high silica range of 63 to 73 wt.% (Figs. 7C, D). One gabbro, AZR1 (Ishihara and Murakami, 2006), is very high in MgO (12.5 wt.%), implying high magnesian source rock in the upper mantle for this rock. About zinc (Zn^{2+}, 0.75Å) replacing ferrous iron (Fe^{2+}, 0.78Å) and Mg^{2+} (0.72Å), the contents are similar to the average content of the Okueyama pluton but variable at the low silica range rocks (Fig. 7E). About copper (Cu^{2+}, 0.73Å), the contents are generally higher in mafic rocks but are lower in the high silica range rocks than the average of the Okueyama granitoids (Fig. 7F).

Among the other trace element, characteristics of the Cape Ashizuri pluton are abundance of HFSE (high-field-strength elements), notably Zr, Hf, Nb, Ta, Y, REE, Th and U, and also F. The HFSE-bearing accessory minerals occur generally as euhedral forms scattered in the rock-forming minerals, but fluorite, the source of fluorine, is typically seen as rounded forms associated with mafic silicates, especially of biotite.

The Zr contents show unique distribution pattern.

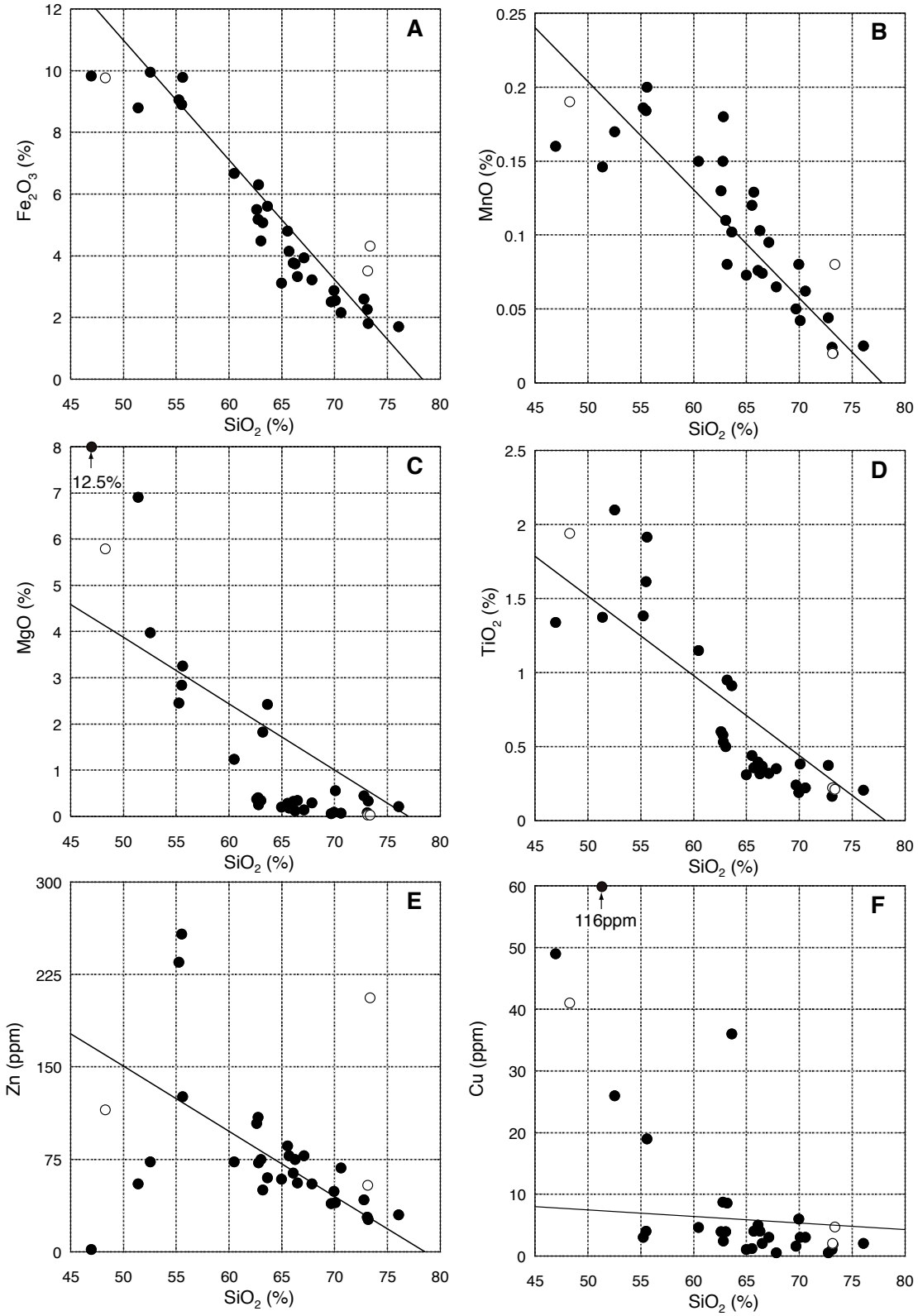

Fig. 7 Harker diagrams for Fe_2O_3, MnO, MgO, TiO_2, Zn and Cu.

They are low at low-silica range and are highest around 66 wt.% SiO_2, then decrease to the higher silica contents (Fig. 8A). The highest values were obtained on 58A142 and drill-core samples (solid triangle).

As a whole, Zr contents are the highest at 65-67 wt.% SiO_2 rocks, similarly to the pattern observed in the Boggy Plain pluton of the Lachlan Fold Belt, Southeast Australia, which was considered as one of the

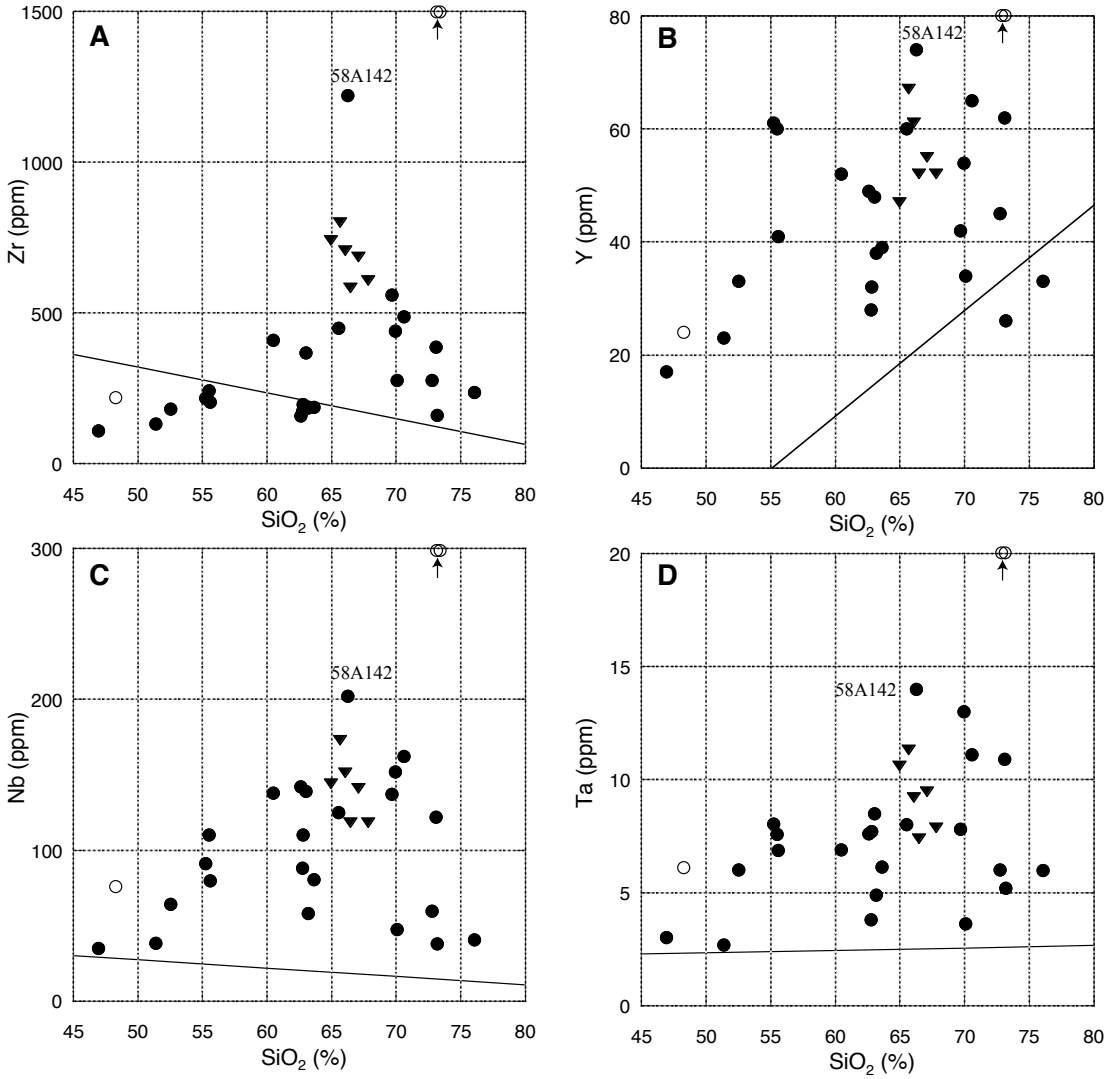

Fig. 8 Harker diagrams for Zr, Y, Nb, and Ta. Solid triangle for the six drill core samples for Figs. 8 and 9.

typical patterns for the high temperature I-type granites (Chappell *et al.*, 2004). The whole contents of Zr are much higher than the average of the Okueyama granitoids, which agree to the experimental data implying that solubility of zircon is much higher in peralkaline melt than metaluminous or peraluminous melt (Linnen and Keppler, 2002). The highest content is 1,220 ppm, which is the highest among the Japanese granitoids.

Contents of Y, Nb and Ta are high and are similar to that of Zr (Figs. 8B, C, D). The contents are much higher in the Cape Ashizuri granitoids than in the Okueyama granitoids (Figs. 8B, C), which agrees to alkalinity control of solubility of $MnNb_2O_6$ in granitic melts (Linnen and Keppler, 1997). Again, the highest peaks are around 66 wt.% SiO_2 (Fig. 8C). Distribution of Ta is very similar to that of Nb in the Harker diagram (Fig. 8D) for similar ionic radius and charge (Nb^{+5}, 0.69Å, Ta^{+5}, 0.68Å). In all the Zr, Y, Nb, and Ta diagrams, the post-plutonic rhyolite dikes are very high in these elements plotted at the outside of the diagrams.

Both Th and U contents are much higher than the averages of the Okueyama granitoids, and increase with increasing silica contents (Figs. 9A, B). Both La and Ce contents are lower than the averages of the Okueyama pluton at gabbroic composition, but are higher than the averages in the high-silica rocks, with the highest peak at 66 wt.% SiO_2 (Figs. 8E, F), similarly to the patterns of Zr and Nb.

3.2 Binary diagrams

Binary diagrams were made on Zr and other related elements. Zirconium in igneous rocks is contained in zircon ($ZrSiO_4$); zircon forms a complete solid solution with hafnon (Linnen and Keppler, 2002). Therefore, Zr (Zr^{+4}, 0.72Å) - Hf (Hf^{+4}, 0.71Å) pair has the highest correlation coefficient of R = 0.98 (Fig. 10A). Hoshino *et al.* (2010) analyzed zircon from monzogranite phase (No. 152) of the northern part of the plutonic body, and found that the core has 0.93 wt.% HfO_2 but the rim contains 1.94 wt.% HfO_2, implying that hafnon com-

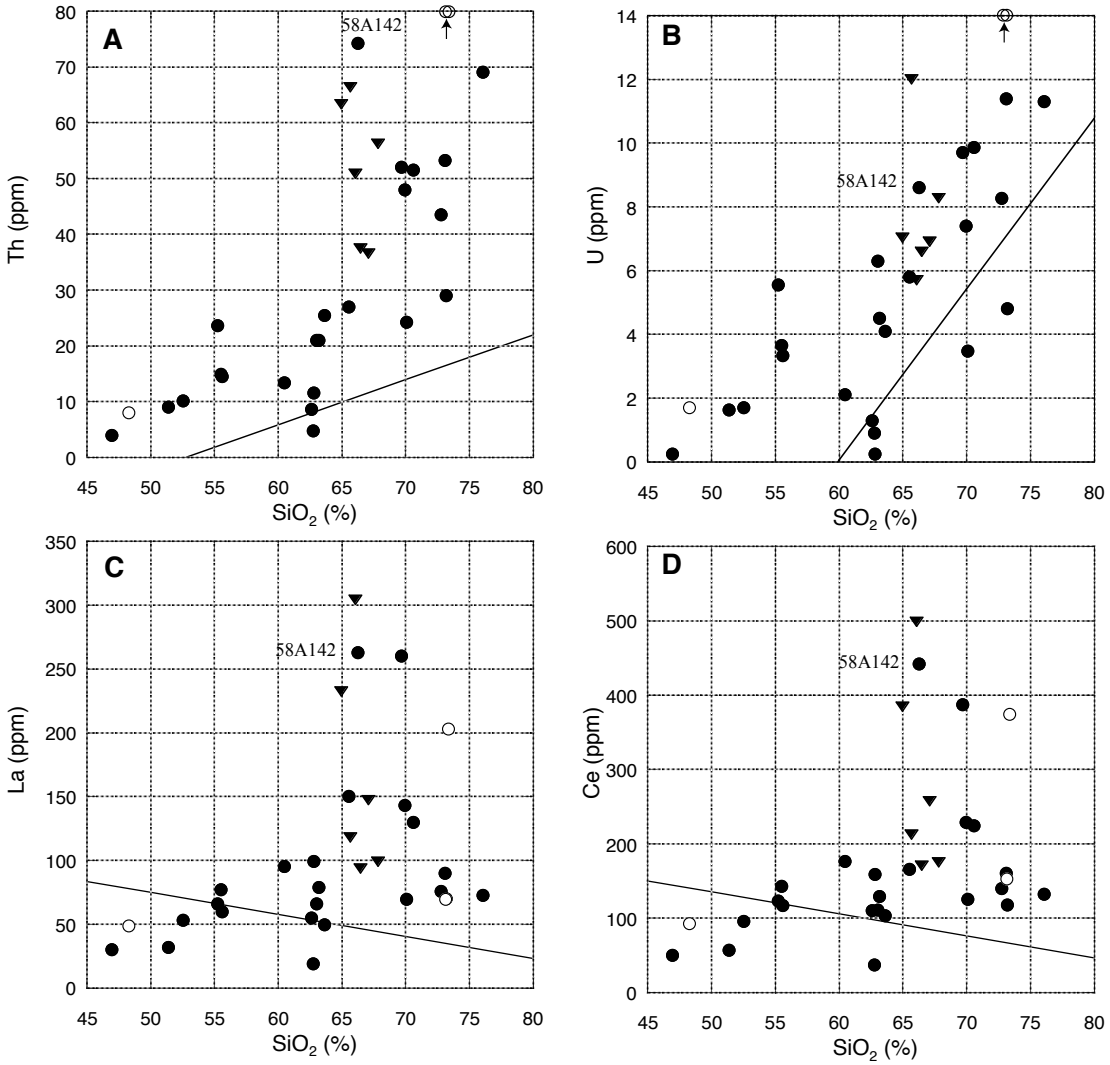

Fig. 9 Harker diagrams for Th, U, La, and Ce. Six drilled samples are shown by solid triangle.

ponent tends to be concentrated in a later zircon phase. Generally speaking, the core of given zircon is concentrated by 0.19 wt.% Y_2O_3, 0.21 wt.% Yb_2O_3, 0.12 wt.% FeO, 0.31 wt.% ThO_2 and 0.43 wt.% UO_2 (Hoshino *et al.*, 2010).

Correlation coefficient of the bulk Zr with Ce is the next high as R = 0.83 (Fig. 10B), which can be expected from the patterns in the Harker diagrams of Figures 8A and 8B. The LREE components should be contained not in zircon but other accessory minerals, such as allanite, monazite and titanite. The correlation coefficients of Zr with Nb, Th, Y and U are lower as 0.79, 0.76, 0.71 and 0.59, respectively. Niobium was detected in ilmenite up to 4.4 wt.% Nb_2O_3 by Nakashima and Imaoka (1998). They also recognized in the studied pluton trace amounts of Nb-oxide such as fergusonite, samarskite, columbite and pyrochlore, which could contain some other elements as Y, Ce, Ta, Fe and Ti. Both Th and U are contained in zircon, but their correlation coefficient against Th and U are as low as R = 0.76 (Fig. 10E) and 0.59 (Fig. 10F), respectively.

Among the other heavy elements, the highest correlation coefficient of 0.99 is seen on the La-Ce pair (Fig. 11B), La-Nd (Fig. 12A) and HREE-Dy (Fig. 12C). The high correlation coefficients are observed in Y-Dy (0.97, Fig. 12D), Th-U (0.90, Fig. 11D), Nb-Ta (0.88, Fig. 11A), and Nb-Y (0.83, Fig. 11C). The correlation coefficient of La-Dy pair is only 0.63 (Fig. 12B), implying LREE and HREE occur rather independently depending upon the host REE-bearing minerals.

3.3 REE contents and REE patterns

REE contents of the studied samples are listed in Table 1. The total REE contents vary from 141 ppm of gabbro to 1,046 ppm of the quartz syenite of the drill-core sample at -145.2 meter (DH145.2). Y content is the highest (74 ppm) in the highest Zr rock of 58A142. LREE/HREE ratio is as low as 8.0 to 9.0 in the mafic rocks, but increase in quartz syenite and monzogranite up to 23.1 (DH96.3). Eu anomaly is generally absent

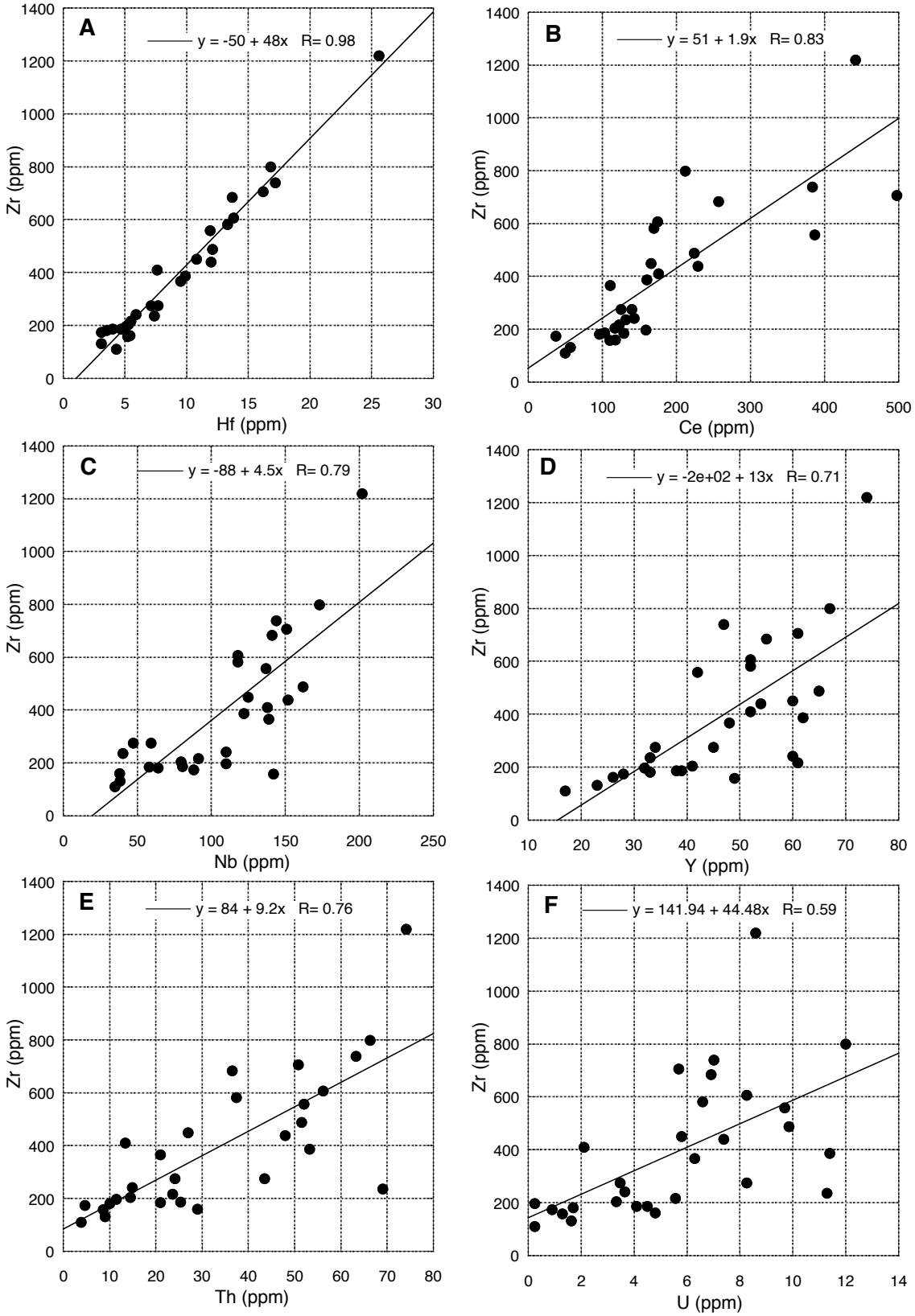

Fig. 10 Binary diagrams for Zr vs. Hf, Ce, Nb, Y, Th and U. Straight line implying the best fit line. The correlation coefficient is also shown.

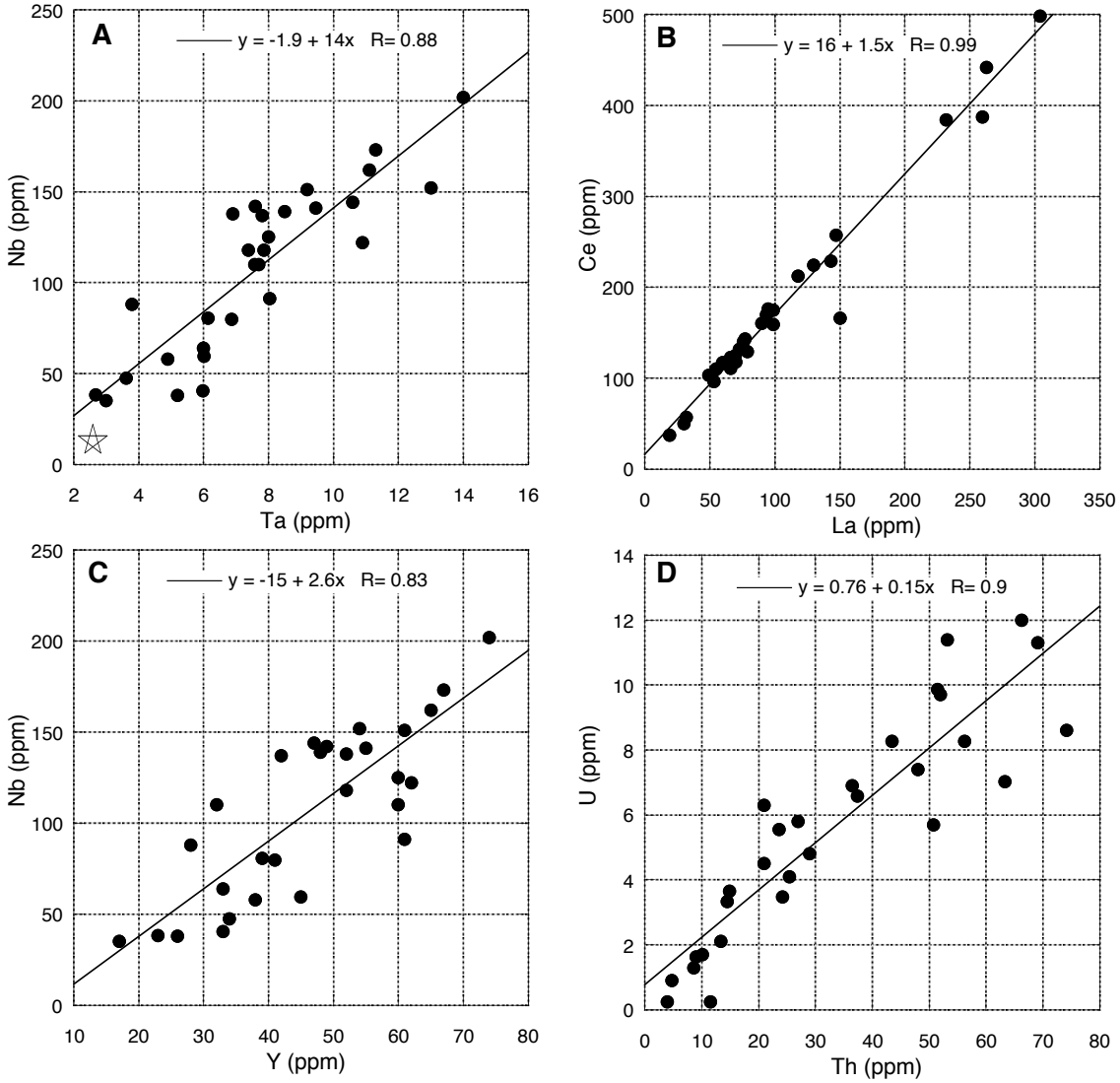

Fig. 11 Binary diagrams for Nb-Ta, Ce-La, Nb-Y and U-Th. Straight line implying the best fit line. The correlation coefficient is also shown.

below 55 wt.% SiO_2 but is seen above this value.

REE pattern of the studied rocks are shown in Figures 13 A to D. The 58A102 gabbro shows the lowest and flat pattern (Fig. 13A). In increasing with silica and potassium contents, the REE contents increase and the negative Eu anomalies also increase. The 58A142 sample with 66.3 wt.% SiO_2 has the largest negative Eu anomaly (Fig. 13A). The same is also seen on the 58A124 point where two mafic monzonites with 55.2-55.5 wt.% SiO_2 mingled with felsic quartz syenite with 70.6 wt.% SiO_2. The monzonites have no but quartz syenite has Eu-negative anomaly (Fig. 13B). It could mean that Ca^{2+} of an early crystallized plagioclase was substituted by Eu^{2+}, thus stayed in mafic counterpart left behind at depth.

Quartz syenites from the drill core have the highest REE contents and the largest negative Eu anomaly (Fig. 13C), including 58A152 monzogranite which intrudes into gabbroids near the Cape Ashizuri. They are considered to have generated from mafic igneous source rocks by small degrees of partial melting. In the other high silica rocks of monzogranite (58A118, 58A130 and 69AZ01), their REE patterns are similar to those of the quartz syenite (Fig. 13D), but they occur in the northernmost part of the Cape Ashizuri pluton and interacted with the intruded Shimanto sedimentary rocks. They have lower NK/A ratio and are lower in the REE contents. These granites may have been formed by interaction between the quartz syenitic magma and partial melting of the sedimentary wall rocks.

Feldspars in igneous rocks have large positive Eu-anomalies. The Eu-anomaly of plagioclase decreases with increasing fO_2 and increasing temperature (Hanson, 1980). This means that Eu is divalent in a reduced magma and preferentially replaces Ca^{2+} position in plagioclase. In Figure 13A, the rock of 51.4 wt.% SiO_2 has no and the rocks of 55.6 and 63.6 wt.% SiO_2 have small Eu-anomalies, but the rocks of 66.3-76.1

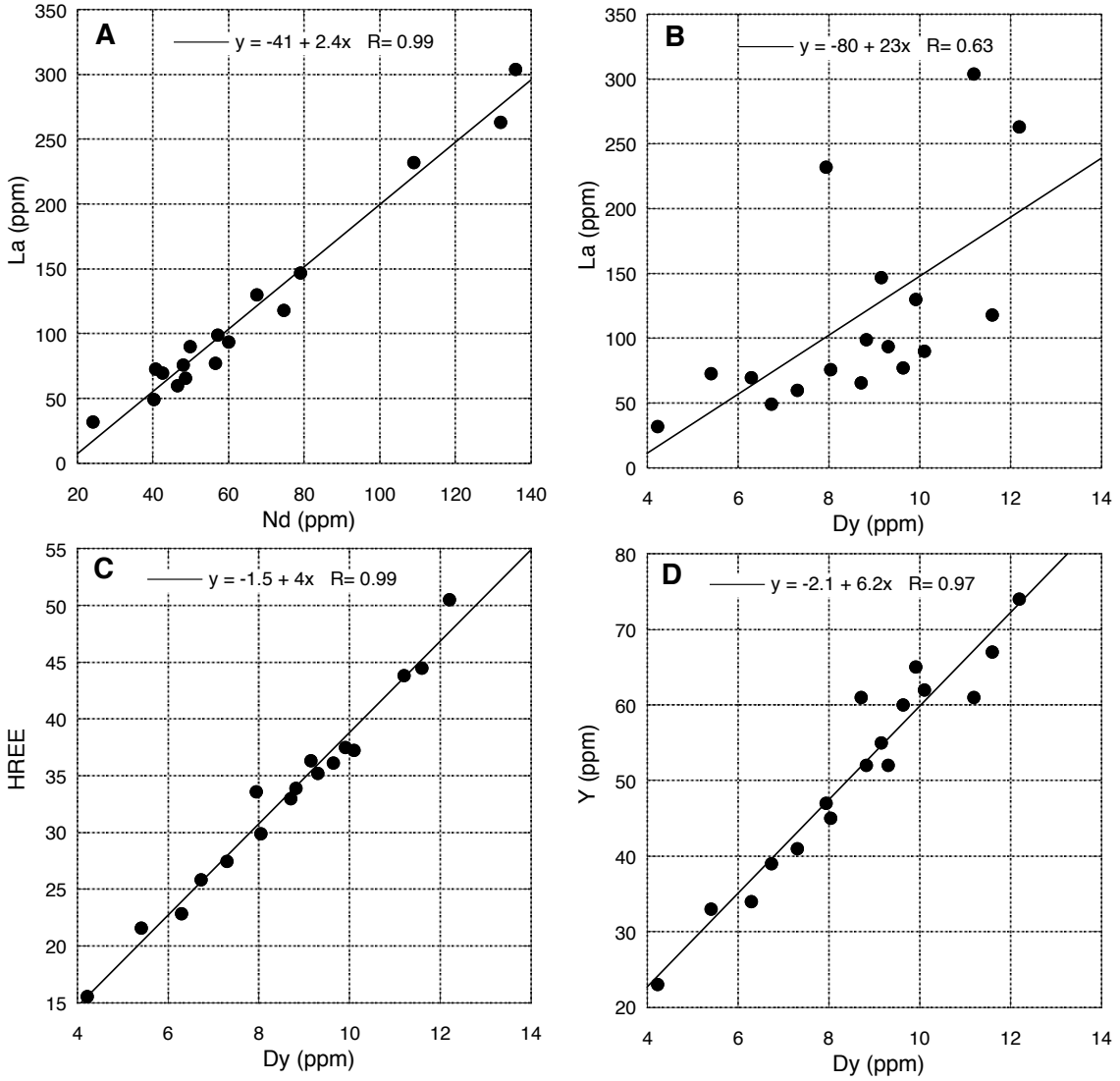

Fig. 12 Binary diagrams for La-Nd, La-Dy, HREE-Dy and Y-Dy. Straight line implying the best fit line. The calculated correlation coefficients are also shown.

wt.% SiO_2 have a distinct Eu-negative anomaly. These could be interpreted that Eu was enriched in calcic plagioclase crystals of calcic and mafic magmas, which crystallized at depth and left behind when the alkaline granitoids intruded upward.

4. Chemical compositions of selected rare minerals

The Cape Ashizuri granitoids are characterized by many rare accessory minerals, and zircon and titanite may be visible by naked eyes. Besides euhedral crystals, zircon shows many strange textures, which may be due to resorption and other reasons. Hayashi and Akai (2011) studied zircon from two localities of quartz syenite and granite, and classified its textures into three types, as Resorption disturbance, Local disturbance, and Hafnon-like disturbance. Ti-rich ferriallanite was studied by Nagashima *et al.* (2011).

Thorite and uranothorite can be found radiometric survey (Hayashi *et al.*, 1969), and Zn- and Nb-ilmenite, and columbite, euxenite, fergusonite, samarskite, and a pyrochlore-like mineral occur in syenite (Nakashima and Imaoka, 1998). We also studied accessory minerals of the quartz syenite with the highest Zr content (58A142) and a moderate one (DH96.3) and one monzogranite (58A124F), and analyzed Mn- and Nb-ilmenite, zircon, allanite, titanite, fergusonite and chevkinite by an electron probe microanalyzer (EPMA) with the method described in Hoshino *et al.* (2006, 2010). The results are shown in Tables 2 to 7.

4.1 Ilmenite

Ilmenite is commonly contained in both ilmenite-series and magnetite-series granitoids. The ilmenites in ilmenite-series granitoids of the Outer Zone granites (Osumi and Takakumayama plutons) have MnO contents of 5 to 19 wt.%, which tends to increase toward

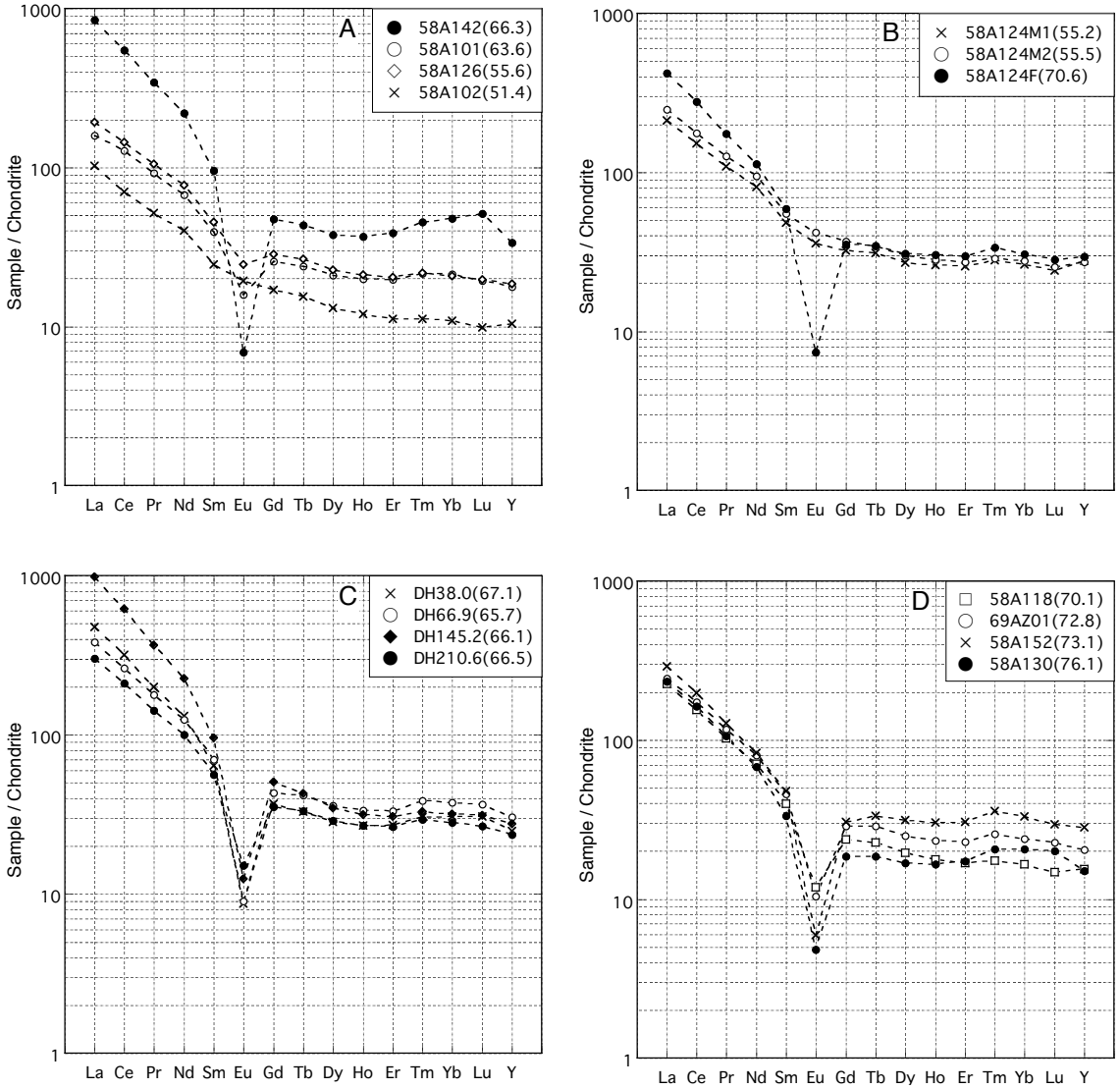

Fig. 13 Selected REE patterns of the studied plutonic rocks.

the margin of crystals (Tsusue, 1973). Tsusue and Ishihara (1974) found common occurrences of hemo-ilmenite in the magnetite-series granitoids in the Sanin Belt of the Inner Zone of SW Japan, but no such minerals are observed in the Ashizuri-misaki magnetite-series granitoids, implying relatively lower oxygen fugacity of the Cape Ashizuri pluton than typical magnetite-series granitoids.

In the Cape Ashizuri body, Nakashima and Imaoka (1998) reported 1.8 to 4.6 wt.% MnO and up to 4.4 wt.% Nb_2O_5 in the ilmenites of the quartz syenite, where Nb is substituting octahedral site of Ti. Our results are shown in Table 2. MnO contents are as high as 4.3-5.7 wt.% in the 58A142 quartz syenite, but as low as 1.7-1.8 wt.% in the DH96.3 quartz syenite. The 58A124 monzogranite has intermediate values of 2.2 and 2.4 wt.% MnO.

The Nb_2O_5 contents are higher, 2.0 to 3.8 wt.% , in the quartz syenites than 0.27 wt.% of the 58A124 monzogranite (Table 2). The high value is seen at rim of ilmenite crystals, which implies that the niobium was added during the latest magmatic stage of the magma crystallization.

4.2 Zircon

Zircons of the granitic terrains in Japan were studied by Hoshino *et al.* (2010), and classified into (HREE)-U-Th-poor type 1, which is hosted in granitoids themselves, and HREE-U-Th-rich type 2, which occurs generally in granitic pegmatites. Within the type 1, zircons are composed of (A) low REE-Th-U subtype and (B) high REE-Th-U-F subtype, the latter of which tends to occur in the well fractionated granites of the Sanyo Sn-W mineralized belt, such as Naegi Granite, Tanakami Granite, and Kurashiki Granite of southern Okayama Prefecture (Ishihara and Murakami, 2006).

Zircons from the Cape Ashizuri pluton are charac-

Table. 2 Chemical composition of ilmenites of selected monzogranite and quartz syenites.

Sample no.	58A124F: monzogranite		58A142: quartz syenite				DH96.3: quartz syenite			
Spot Loc.	1. core		1. core		2. rim		1. core		2. rim	
n	7	100%	4	100%	2	100%	2	100%	4	100%
TiO_2	45.30	49.18	43.97	46.26	41.45	43.62	43.26	45.38	42.80	44.94
FeO	44.18	47.96	44.71	47.03	43.96	46.26	47.72	50.06	48.20	50.61
MnO	2.16	2.35	4.27	4.49	5.72	6.02	1.78	1.87	1.74	1.82
CaO	0.20	0.22	0.07	0.07	0.07	0.07	0.03	0.04	0.01	0.01
Nb_2O_5	0.27	0.29	2.04	2.15	3.84	4.04	2.52	2.65	2.50	2.62
Total	92.11	100.00	95.06	100.00	95.03	100.00	95.33	100.00	95.24	100.00

Table. 3 Chemical composition of zircons of selected monzogranite and quartz syenites.

Sample No.	58A124F: monzogranite				58A142: quartz syenite				DH96.3: quartz syenite				
	Euhedral crystal		Corroded crystal		Corroded	Euhedral crystal		Euhedral	Zoned		X	Y	Z
Spot Loc.	1. core	2. rim	1. core	2. rim		Bright	Dark		Dark	Bright	Single phase crystals		
n	2 (1, 2)	2 (3, 4)	2 (5,6)	2(7,8)	3(9–11)	2 (12,14)	2 (13,15)	2(16,17)	2(18–19)	2(20–21)	3(22–24)	2(25–26)	2(27–28)
SiO_2	34.19	34.09	33.90	33.60	34.93	34.07	34.61	34.57	35.25	35.75	34.69	35.15	35.40
ZrO_2	62.95	61.06	62.88	61.26	64.69	62.75	64.19	64.33	65.09	62.00	63.53	65.40	65.03
HfO_2	2.36	2.47	1.45	1.90	1.36	1.09	1.32	1.03	1.45	1.62	1.08	1.43	1.02
Y_2O_3	0.17	0.67	0.53	0.90	0.12	1.00	0.37	0.26	0.06	0.08	0.56	0.07	0.11
Total	99.67	98.29	98.76	97.65	101.10	98.91	100.49	100.19	101.84	99.46	99.86	102.05	101.56
HfO_2/ZrO_2*100	3.75	4.06	2.30	3.10	2.10	2.61	2.06	1.61	2.23	2.61	1.70	2.19	1.57
Y_2O_3/ZrO_2*1000	2.70	11.00	5.40	14.70	1.90	1.13	5.76	3.98	0.92	12.74	8.82	1.07	1.69

Table. 4 Chemical composition of allanites of selected quartz syenite.

Sample No.	58A142: quartz syenite					DH96.3: quartz syenite	
Spot Loc.	G, 1–5	G, 6–7	G, 8–9	10–14	H, 15–18	I, 19–23	24–25
n	5	2	2	5	4	5	2
SiO_2	31.50	30.86	30.99	31.36	31.19	31.33	30.25
TiO_2	3.08	3.71	3.92	2.73	2.63	3.14	3.17
Al_2O_3	8.97	7.43	7.29	9.44	9.24	9.93	9.38
FeO	19.56	20.30	20.50	19.42	19.81	18.49	18.32
MnO	0.37	0.36	0.41	0.42	0.44	0.32	0.29
CaO	9.53	8.99	9.10	9.66	9.55	9.64	9.41
La_2O_3	7.95	8.27	7.84	7.61	7.93	7.61	8.24
Ce_2O_3	12.92	13.09	12.96	12.95	13.09	12.54	12.26
Pr_2O_3	1.08	0.94	1.10	1.20	1.08	0.95	0.99
Nd_2O_3	2.92	2.75	3.00	3.18	3.18	2.83	2.60
Total REE	25.38	25.81	25.50	25.41	25.74	24.58	25.23
ThO_2	0.16	0.38	0.54	0.17	0.05	0.57	0.54
Total	98.04	97.07	97.63	98.13	98.19	97.35	95.42

For G to I, see Plate II

Table. 5 Chemical composition of titanites of selected quartz syenite.

Sample No.	58A124F: monzogranite			
Spot Loc.	1	2	3 core	3 rim
n	3	5	3	2
SiO_2	30.29	30.52	29.99	30.02
TiO_2	30.73	30.14	29.71	28.78
Al_2O_3	2.49	2.79	2.44	1.60
FeO	1.52	1.65	1.72	2.50
CaO	34.18	34.03	33.20	32.72
La_2O_3	0.03	0.03	0.09	0.05
Ce_2O_3	0.20	0.18	0.45	0.41
Pr_2O_3	0.02	0.04	0.04	0.07
Nd_2O_3	0.04	0.06	0.21	0.14
ThO_2	0.02	0.04	0.04	0.01
Y_2O_3	0.07	0.06	0.16	0.21
ZrO_2	0.19	0.18	0.18	0.10
Nb_2O_5	0.29	0.31	0.71	2.70
Total	100.06	100.02	98.95	99.31

terized by their abundance and ragged shapes, which could be euhedral zircons broken, resorped and/or corroded in later stages (A-F, Plate II). These zircons belong to the subtype A of the type 1 by Hoshino *et al.* (2010), because REE, U and Th are below the detection limits (Table 3), but yttrium is contained up to 1.0 wt. % Y_2O_3. The Y-bearing phase is seen brighter than Y-free phases. Yttrium tends to be depleted in the core and enriched in the rim (see Table 3); $Y_2O_3/ZrO_2 \times 1{,}000$ of the core zircon ranges from 1.57 to 3.75, while the rim zircon varies from 2.7 to 14.7. This mode of occurrence indicates that the yttrium was added into the zircon crystals from the remaining fluid phase in the latest magmatic stage.

The most common impurity in the zircons is hafnium, which goes up to 2.42 wt.% HfO_2. Hafnium tends to be rich in the core of single crystal, indicating its closest geochemical affinity with zirconium. The $HfO_2/ZrO_2 \times 100$ ratio varies from 1.61 to 3.75 in the main

Table. 6 Chemical composition of fergusonites of the 58A142 quartz syenite.

Sample No.	58A142: quartz syenite					
Spot Loc.	core: 1–3	rim; 4–5	core,6–7	rim, 8–9	10, 11	12, 13
n	3	2	2	2	2	2
SiO_2	4.40	8.04	5.21	2.60	4.23	0.48
TiO_2	0.76	0.14	0.94	0.35	0.91	0.94
FeO	2.11	5.09	2.29	0.66	1.55	0.31
CaO	1.43	2.52	1.46	1.72	1.53	2.22
La_2O_3	0.41	0.13	0.39	0.19	0.33	0.54
Ce_2O_3	2.18	0.86	2.46	2.18	2.19	3.17
Pr_2O_3	0.47	0.19	0.47	0.63	0.42	0.76
Nd_2O_3	2.77	2.40	2.92	4.47	3.15	3.61
Sm_2O_3	1.25	1.80	1.35	2.33	1.44	1.35
Gd_2O_3	2.75	3.91	3.00	4.21	2.97	2.90
Tb_2O_3	0.36	0.54	0.46	0.53	0.41	0.36
Dy_2O_3	2.85	3.49	3.05	3.30	2.61	2.86
Er_2O_3	1.74	1.85	1.73	1.66	1.50	1.80
Yb_2O_3	1.40	2.48	0.98	1.96	1.33	1.51
Lu_2O_3	0.34	0.60	0.28	0.53	0.34	0.41
Ta_2O_5	1.17	1.18	0.77	1.21	0.83	0.84
Y_2O_3	13.52	18.20	13.40	16.70	13.13	16.99
Nb_2O_5	42.77	38.40	39.30	44.36	41.70	46.38
ThO_2	4.84	1.85	7.22	4.43	7.64	6.98
UO_2	4.31	1.45	3.13	1.61	2.93	3.24
Total	91.84	95.11	90.81	95.60	91.14	97.66

Table. 7 Chemical composition of chevkinite of the 58A142 quartz syenite.

Sample No.	58A142		
Spot Loc.	1–2	3–4	5–6
n	3	3	2
SiO_2	20.63	20.59	20.56
TiO_2	14.70	15.05	14.35
Al_2O_3	0.46	0.45	0.46
FeO	11.87	11.66	11.75
CaO	4.18	4.34	3.89
La_2O_3	12.47	12.77	12.48
Ce_2O_3	20.96	21.05	21.19
Pr_2O_3	1.66	1.51	1.63
Nd_2O_3	5.56	5.37	5.57
Y_2O_3	0.45	0.39	0.37
ZrO_2	0.62	0.78	0.46
Nb_2O_5	2.82	2.58	3.29
ThO_2	1.40	1.19	1.24
Total	97.80	97.72	97.24

phase of the zircon crystals.

4.3 Allanite

Allanites occur in anhedral forms in the studied granitoids (G-I, Plate II). This mineral in granitic rocks are known to have MnO-poor chemistry, less than 2 wt.% MnO, in the magnetite-series granitoids, while MnO-rich ones, more than 2 wt.% MnO, are common in the ilmenite-series granitoids (Hoshino *et al.*, 2006). The MnO-poor allanites are relatively rich in LREE, while the MnO-rich ones tend to have enrichment in middle rare earth elements (MREE). This relationship is expressed by the coupled substitution [Mn^{2+} + (MREE, $HREE^{3+}$) = Ca^{2+} + $LREE^{3+}$] (Hoshino *et al.*, 2006).

Allanites were found in two quartz syenites, zircon-rich one (58A142) and drill core sample (DH96.3); the both belong to MnO-poor type due to low MnO content (<0.44 wt.% MnO). This is consistent with the host granitoid belonging to a magnetite series. Allanites in these quartz syenites are very rich in LREE; the total rare earth contents of LREE range from 25.4 to 25.8 wt.% on the 58A142 quartz syenite, and 24.6 to 25.2 wt.% on the DH96.3 quartz syenite (Table 4). On the other hand, thorium content varies greatly from 0.05 to 3.7 wt.% ThO_2 for the 58A142 quartz syenite, depending upon grains.

4.4 Titanite

Coarse-grained euhedral titanites are commonly seen in felsic phase of the magma mingled part at the 58A124 locality. Their analyzed crystals are shown in Plate III and chemical compositions are indicated in Table 5. The chemical compositions are rather homogeneous, but one euhedral crystal has a bright rim rich in FeO, LREE, Y_2O_3 and Nb_2O_5 (C in Plate III), which is the latest crystallized phase of the magmatic fractionation. Thus, these components are considered to have added during the latest stage of the solidification.

4.5 Fergusonite and chevkinite

Fergusonite is seen in the 58A142 quartz syenite. This mineral occurs as anhedral crystals (D-F in Plate III), having brighter rims (e.g., E in Plate III). The compositions are heterogeneous, depending upon crystals as seen in Table 6. In the core vs. rim variations, Th, U and LREE are depleted in the rim of fergusonite, while HREE and Y are enriched in the rim.

Chevkinite was first found in Japan by Imaoka and Nakashima (1994) in quartz syenite of this pluton. We also identified this mineral in the zircon-rich rock of the 58A142 quartz syenite, and its chemical compositions are shown in Table 7. A distinct difference between the two results is seen on the thorium contents; Imaoka and Nakashima (1994) reporting 4.84 wt.% ThO_2.

5. Genetic consideration on the Cape Ashizuri pluton

Miocene alkaline body of the Cape Ashizuri is composed of both quartz undersaturated and oversaturated igneous rocks, similarly to other alkaline rock province (e.g., Oslo region, Neumann ,1980). They are composed of gabbroic and granitic rocks in both the main plutonic stage and post-plutonic subvolcanic stages, as mentioned previously. The lowest silica rock is 47.0 wt.% SiO_2, which contains 12.5 wt.% MgO (AZR1,

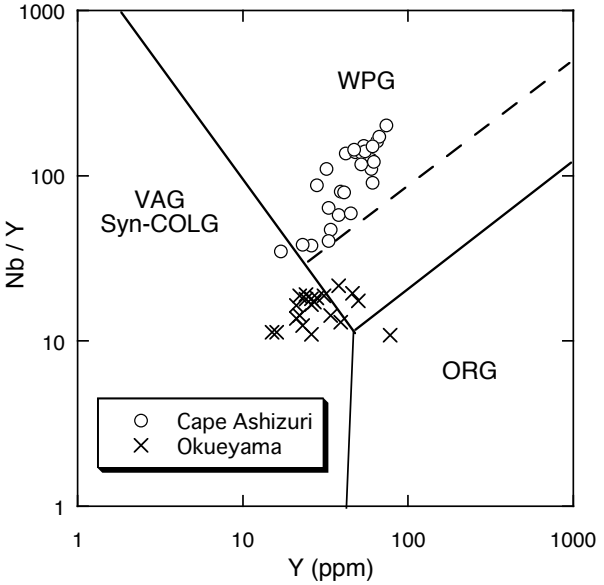

Fig. 14 Nb/Y vs. Y plot of the Cape Ashizuri and Okueyama plutonic rocks.

Ishihara and Murakami, 2006). This rock must have originated from a deep and mafic source rock in the upper mantle, and therefore moved upward invading through the subducting Philippine Plate, mafic lower crust and overlying accretionary complex of the Shimanto Supergroup during a certain period of the Miocene time, having severe interaction locally with the magmas from crustal sources.

All the other Miocene granitic rocks in the Outer Zone belong to the ilmenite-series composed of both I- and S-types. Some amounts of the sedimentary rocks of the accreted prism were considered mixed with the magmas from the depth; thus formed I- or S-type magma depending upon their mixing ratio. The Okueyama granodiorite-granite pluton is one typical example of I-type ilmenite-series having the exposure of 96 km^2. If these granitoids are plotted on the Nb/Y vs. Y diagram to discriminate their tectonic settings (Fig. 14), the Cape Ashizuri granitoids stay in the within-plate-granite (WPG) area, but the Okueyama granitoids are located mostly in the volcanic arc granite (VAG) area, although the two plutons occur in typical volcanic arc setting.

The Okueyama granitic body is vertically zoned being granodiorite at the lowest part and changing its composition upward to monzogranite, then aplitic granite containing pegmatite at the top 200 m, and thus differentiated vertically (Takahashi, 1986). They are composed of quartz-oversaturated rocks, except for a small part at 680 m above sea level, which is composed of monzonite (MT680, see Appendix I of Ishihara and Chappell, 2010). The Cape Ashizuri pluton, on the other hand, is horizontally zoned being alkaline monzosyenitic rocks in the southern part and quartz oversaturated monzogranite in the northern part, and the gabbroids occurring between them (Fig. 2). They are considered products of different intrusive bodies but genetically related.

The gabbroic rock with the lowest silica of 47.0 wt.% SiO_2 and highest magnesium as 12.5 wt.% MgO, has the alkali contents of 2.25 wt.% Na_2O and 1.23 wt.% K_2O, thus belonging to an alkaline gabbroid. Alkaline granitoids can be differentiates of the alkaline gabbroid, if much larger host gabbroid hidden underneath the present body. Another possibility, which seems more probable, is small degree of partial melting of igneous lower continental crust below the Shimanto accretionary complex by the heat brought up by the alkaline gabbroic magma. Because degree of the melting was small, alkaline feldspar components of alkalis and gallium, also fluorine moved selectively to the melt phase, and thus Ga-F-rich alkaline granitic magma was formed. Experimentally, zircon solubility is strongly enhanced by addition of $NaSi_3O_7$ to water. The same may be expected on K-silicate. Thus, the alkaline-rich magmas tend to contain abundant zirconium.

High-field strength elements (HFSE) such as Zr, Hf, Nb, Ta, Y, REE and W, are generally concentrated in residual melts during solidification of granitic magmas, as the best observed in the aplitic dike of the Naegi Granite (Ishihara and Murakami, 2006). It means that when the syenitic magma was generated in the lower continental curst below the Cape Ashizuri, the HFSE-rich melt, together with much fluorine, must be the first one to move to the melt phase together with some feldspar components. Thus, the HFSE-rich alkaline granitoids were formed.

The northern half of the Cape Ashizuri pluton is a quartz-oversaturated monzogranite having abundant modal quartz but low Ga contents less than 19 ppm. Thus, it is normal ilmenite-series granite having low magnetic susceptibility, similarly to the other ilmenite-series granitoids of the Outer Zone whose interaction with the accreted sediments are best shown by elevated $\delta^{18}O$ values (Ishihara and Matsuhisa, 1999). Sedimentary blocks and enclaves from the Shimanto accretionary complex are commonly observed in this granite area. This could be intermingled part at depth of the alkaline granitic magma with the shale and sandstones of the accretionary complex, which may have been stacked more than 10 km along the Outer Zone. Presence of sedimentary enclaves and higher initial Sr isotopic ratio support that interpretation.

6. Economic evaluation of the REE-rich granites

Similar REE and Zr-rich alkaline granites occur sporadically in many places in the world. Since these granites have A-type characteristics, they occur generally in an-orogenic environment like in Nigeria (Kinnaird *et al.*, 1985), Namibia (Schmitt *et al.*, 2002), Thor Lake in Canada (Ishihara and Watanabe, 2007) and Baerzhe of the Inner Mongolia (Ishihara and Murakami, 2007),

yet they are seen also in orogenic environment like the studied Cape Ashizuri complex and Bokan Mountain complex in Alaska (Philpotts *et al.*, 1994).

The Bokan Mountain complex of Jurassic age (151-171 Ma) occurs as intrusive rocks in the early Paleozoic accretionary complex of eugeosynclinal sediments in the southeastern Alaska. It has a circular form with 6 km diameter, composed of aegirine granite porphyry at margin and riebeckite granite porphyry in the center (Thompson *et al.*, 1982). The U-Th-REE mineralization is associated with the first collapse of the ring dike formation. The ore deposits occur in pipe-like bodies, as lenses in sheared zones and in vein quartz.

Economically more important REE-rich alkaline granites occur in anorogenic environments in Saudi Arabia, Mongolia and Canada. These granites are rich in Zr, Y, and REE. Microgranite-hosted Ghurayyah type may be the highest in HREE contents (Drysdall *et al.*, 1984). Many of these REE-rich granites have received REE enrichment by both magmatic and hydrothermal processes (Kovalenko *et al.*, 1995; Salvi and Williams-Jones, 2005). It is interesting to find hydrothermal alteration zones in and around the Cape Ashizuri plutonic and subvolcanic bodies.

7. Conclusions

The Cape Ashizuri plutonic complex having an exposed area of 12 km^2 is a unique alkaline plutonic complex, composed of magnetite-series and ilmenite-series granitoids occurring in the Shimanto accretionary sedimentary terrain where all the other Miocene granitic rocks belong to calc-alkaline ilmenite-series granitoids. The Cape Ashizuri plutonic complex has a variety of rock facies, but is grouped into three as (1) gabbroids, (2) alkaline granites with low quartz contents, which are distributed in the southern half of the body, and (3) quartz-oversaturated calc-alkaline monzogranite, exposed in the northern half in contact with the sedimentary wall rocks. These rocks, particularly of alkaline granitoids, are rich in Zr, REE, Nb-Ta, and Th-U, which are contained in the rock-forming minerals of ilmenite, titanite, allanite, fergusonite, chevkinite, uranothorite and others

The alkaline granitoids would have been generated at the lower crust of mafic igneous source rocks by heat brought up by the gabbroic magmas from the upper mantle. A small degree of the partial melting was a main cause to produce HFSE and F dominant magmas. The quartz-oversaturated monzogranite in the northern half would be a mixed magma of the alkaline granitic magma from the depth and local magma generated with interaction of the sedimentary wall rocks of the Shimanto Supergroup.

Acknowledgements: We thank Prof. S. Yoshikura of Kochi University for donation of the most mafic gabbro studied, and Prof. T. Imaoka of Yamaguchi University for providing unpublished rock unit map made in 1993.

References

Chappell, B. W., White, A. J. R., Williams, I. S. and Wyborn, D. (2004) Low- and high-temperature granites. *Proc. Royal Soc. Edinburgh, Earth Sci*., **95**, 125-140.

Cullers, R. L. and Graf, J. L. (1984) Rare earth elements in igneous rocks of the continental crust: Intermediate and silicic rocks – Ore petrogenesis. *Rare Earth Element Geochemistry* (P. Henderson ed.), Elsevier, Amsterdam, 275-316.

Drysdall, A. R., Jackson, N. J., Ramsay, C. R., Douch, C. J. and Hackett, D. (1984) Rare element mineralization related to Precambrian alkali granites in the Arabian Shield. *Econ. Geol*., **79**, 1366-1377.

Hanson, G. N. (1980) Rare earth elements in petrogenetic studies of igneous systems. *Ann. Rev. Earth Planet. Sci*., **8**, 371-406.

Hayashi, H. and Akai, J. (2011) Unusual internal textures and trace element chemistry of zircon from Cape Ashizuri Ring Complex, Kochi, SW Japan. *Petrol. Mineral*., **40**, 1-12 (in Japanese with English abstract).

Hayashi, S., Ishihara, S. and Sakamaki, Y. (1969) Uranium in the decomposed granitic rocks at the Cape Ashizuri, Kochi Prefecture, with special reference to the green uranothorite. *Rept. Geol. Surv. Japan*, no. 232, 93-103 (in Japanese with English abstract).

Hoshino, M., Kimata, M., Shimizu, M., Nishida, N. and Furukawa, T. (2006) Allanite-(Ce) in granitic rocks from Japan: genetic implications of patterns of REE and Mn enrichment. *Can. Mineral*., **44**, 45-62.

Hoshino, M., Kimata, M., Nishida, N., Shimizu, M. and Akasaka, T. (2010) Crystal chemistry of zircon from granitic rocks, Japan: Genetic implications of HREE, U and Th enrichment. *N. Jb. Mineral. Abh*., **187/2**, 167-188.

Iizumi, S. and Murakami, N. (1980) Sr isotopic ratio of the Ashizuri-misaki ring complex. *Abstract Issue for 92nd Annual Mtg., Geol. Soc. Japan*, 338 (in Japanese).

Imaoka, T. and Nakashima, K. (1994) Chevkinite in syenites from Cape Ashizuri, Shikoku Island, Japan. *N. Jb. Mineral. Mh*., **H.8**, 358-366.

Imaoka, T. Nakashima, K. and Murakami, N. (1991) Gallium in A-type granites from the Cape Ashizuri, Kochi Prefecture, Southwest Japan. *Japan. Assoc. Mineral. Petrol. Econ. Geol*., **86**, 354-363 (in Japanese with English abstract).

Ishihara, S. (1979) Lateral variation of magnetic susceptibility of the Japanese granitoids. *Jour. Geol. Soc. Japan*, **85**, 509-523.

Ishihara, S. and Chappell, B. W. (2010) Chemical

compositions of the Miocene granitoids of the Okueyama, Hoei mine and Takakumayama plutons, Outer Zone of SW Japan. *Bull. Geol. Surv. Japan*, **61**, 17-38.

Ishihara, S. and Matsuhisa, H. (1999) Oxygen isotopic constraints on the geneses of the Miocene Outer Zone granitoids in Japan. *Lithos*, **46**, 523-534.

Ishihara, S. and Murakami, H. (2006) Characteristics of REE distribution in granitoid of SW Japan: Miocene plutonic rocks at Ashizuri-misaki and late Cretaceous granitoids of the Sanyo Belt of SW Japan. *Bull. Geol. Surv. Japan*, **57**, 89-103 (in Japanese with English abstract).

Ishihara, S. and Murakami, H. (2007) HREE concentration in the Baerzhe Granites, Inner Mongolia, China. *Resource Geol*., **57**, 137-142 (in Japanese with English abstract).

Ishihara, S. and Watanabe, Y. (2007) Hydrothermal REE deposits: An example of the Thor Lake property. *Resource Geol*., **57**, 65-70 (in Japanese with English abstract).

Ishihara, S., Teraoka, Y., Terashima, S. and Sakamaki, Y. (1985) Chemical variation of Mesozoic-Cenozoic sandstone and shale across the western Shikoku district. *Bull. Geol. Surv. Japan*, **36**, 85-102.

Ishihara, S., Tanaka, T., Terashima, S., Togashi, S., Murao, S. and Kamioka, H. (1990) Peralkaline rhyolite dikes at the Cape Ashizuri: A new type of REE and rare metal mineral resources. *Mining Geol*., **40**, 107-115.

Kinnaird, J. A., Bowden, P., Ixer, R. A. and Odling, N. W. A. (1985) Mineralogy, geochemistry and mineralization of the Ririwai complex, Northern Nigeria. Jour. *African Earth Sci*., **3**, 185-222.

Kovalenko, V. I., Tsaryeva, G. M., Goreglyad, A. V., Yarmolyuk, V. V., Troitsky, V. A., Hervig, R. L. and Farmer, G. L. (1995) The peralkaline granite-related Khaldzan-Buregtey rare metal (Zr, Nb, REE) deposit, Western Mongolia. *Econ. Geol*., **90**, 530-547.

Linnen, R. L. and Keppler, H. (1997) Columbite stability in granitic melts: consequences for the enrichment and fractionation of Nb and Ta in the Earth's crust. *Contrib. Mineral. Petrol*., **128**, 213-227.

Linnen, R. L. and Keppler, H. (2002) Melt composition control of Zr/Hf fractionation in magmatic processes. *Geochim. Cosmochim. Acta*, **66**, 3293-3301.

Mason, B. (1966) *Principles of Geochemistry. 3rd ed*., 329 p.

Murakami, H. and Ishihara, S. (2006) REE geochemistry of weathered soil within Miocene granitoids in the Ashizuri-misaki area, SW Japan: Possibility as REE resources. *Chikyukagaku (Geochemistry)*, **40**, 147-165 (in Japanese with English abstract).

Murakami, N. and Imaoka, T. (1985) Rapakivi granite. *Jour. Geol. Soc. Japan*, **91**, 179-194 (in Japanese with English abstract).

Murakami, N. and Masuda, Y. (1984) Trace elements in the Tertiary igneous rocks from Cape Ashizuri, Kochi Prefecture, Southwest Japan. Japan. Assoc. Mineral. Petrol. *Econ. Geol*., **79**, 318-328.

Murakami, N. and Matsuo, H. (1963) Petrological studies on the metasomatic syenites in Japan. Part 1. Syenites of the Cape of Ashizuri, Kochi Prefecture. Japan. Assoc. Mineral. Petrol. *Econ. Geol*., **50**, 93-109 (in Japanese with English abstract).

Murakami, N., Imaoka, T. and Uozumi, S. (1989) Ring complex of the Cape of Ashizuri, and its mode of emplacement, Kochi Prefecture, Southwest Japan. *In Collapse Basins*. Monogr. 36, Assoc. Geol. Collab., 115-142 (in Japanese with English abstract).

Murakami, N., Kanisawa, S. and Ishikawa, K. (1983) High fluorine content of Tertiary igneous rocks from the Cape of Ashizuri, Kochi Prefecture, Southwest Japan. Japan. Assoc. Mineral. Petrol. *Econ. Geol*., **78**, 497-504 (in Japanese with English abstract).

Nagashima, M., Imaoka, T. and Nakashima, K. (2011) Crystal chemistry of Ti-rich ferriallanite-(Ce) from Cape Ashizuri, Shikoku Island, Japan. *Amer. Mineral*., **96**, 1870-1877.

Nakashima, K. and Imaoka, T. (1998) Niobian and zincian ilmenites in syenites from Cape Ashizuri, Southwest Japan. *Mineral. Petrol*., **63**, 1-17.

Neumann, E. R. (1980) Petrogenesis of the Oslo region larvikites and associated rocks. *Jour. Petrol*., **21**, 499-531.

Philpotts, J. A., Taylor, C. D. and Baedecker, P. A. (1994) Rare-earth enrichment at Bokan Mountain, Southeast Alaska. Geologic Studies in Alaska by the U.S. Geol. Surv., 89-100.

Salvi, S. and Williams-Jones, A. E. (2005) Alkaline granite-syenite deposits. In Linnen, R. and Samson, I., eds., *Rare-element geochemistry and mineral deposits*. Geol. Assoc. Canada, Short Course Notes 17, 315-341.

Schmitt, A. K., Tbumbull, R. B., Dulski, P. and Emmermann, R. (2002) Zr-Nb-REE mineralization on peralkaline granites from the Amis complex, Brandberg (Namibia): Evidence for magmatic pre-enrichment from the melt inclusions. *Econ. Geol*., **97**, 399-413.

Shibano, T. (1958) Un-utilized iron mineral resources in the Ashizurimisaki District. *Un-utilized Mineral Resources No. 5*, Ministry of International Trade and Industry, 168-172 (in Japanese).

Shibata, K. and Ishihara, S. (1979) Initial $^{87}Sr/^{86}Sr$ ratios of plutonic rocks from Japan. *Contrib. Mineral. Petrol*., **70**, 381-390.

Shibata, K. and Nozawa, T. (1982) Radiometric age map of Japan: Granitic rocks. Scale 1:3,000,000. Geol. Surv. Japan.

Shinjoe, H., Orihashi, Y. and Sumii, T. (2010) U-Pb

zircon ages of syenitic and granitic rocks in the Ashizuri igneous complex, southwestern Shikoku: Constraint for the origin of forearc alkaline magmatism. *Geochem. Jour*., **44**, 275-283.

Suzuki, T. (1938) *Explanatory text of the geological map of Japan. Scale 1:75,000, Sukumo* (in Japanese with English abstract).

Takahashi, M. (1986) Anatomy of a middle Miocene Valles-type caldera cluster: Geology of the Okueyama volcano-plutonic complex, Southwest Japan. Jour. *Volc. Geothermal Res*., **29**, 33-70.

Teraoka, Y. (1979) Provenance of the Shimanto geosynclinals sediments inferred from the sandstone compositions. *Jour. Geol. Soc. Japan*, **85**, 753-769

Teraoka, Y., Okumura, K., Suzuki, M. and Kawakami, K. (1999) Clastic sediments of the Shimanto Supergroup in Southwest Japan. *Bull. Geol. Surv. Japan*, **50**, 559-590 (in Japanese with English abstract).

Thompson, T. B., Pierson, J. R. and Lyttle, T. (1982) Petrology and petrogenesis of the Bokan granite complex, southeastern Alaska. *Geol. Soc. America, Bull*., **93**, 898-908.

Tsusue, A. (1973) The distribution of manganese and iron between ilmenite and granitic magma in the Osumi Peninsula, Japan. *Contrib. Mineral. Petrol*., **40**, 305-314

Tsusue, A. and Ishihara, S. (1974) The iron-titanium oxides in the granitic rocks of Southwest Japan. *Mining Geol*., **24**, 13-30 (in Japanese with English abstract).

Wilke, M., Schmidt, C., Dubrail, J., Appel, K., Borchert, M., Kvashnina, K. and Manning, C. E. (2012) Zircon solubility and zirconium complexation in $H_2O + Na_2O + SiO_2 \pm Al_2O_3$ fluids at high pressure and temperature. *Earth Planet. Sci. Letters*, **349-350**, 15-25.

Received August 16, 2012
Accepted March 22, 2013

足摺岬の付加体に貫入するジルコンと希土類元素に富むアルカリ深成岩類

石原舜三・星野美保子

要　旨

西南日本外帯の足摺岬火成岩体は露出面積 12 km^2 の小岩体であるが，その南部は斑レイ岩および狭義の閃長岩・石英閃長岩から閃長花崗岩に至る幅広いアルカリ花崗岩類，その北部は四万十帯に接する石英に富む黒雲母モンゾ花崗岩で構成される複合岩体である．化学分析値をハーカー図上で検討すると，黒雲母モンゾ花崗岩の 3 個を除き A/CNK<1.0, 即ちメタアルミナスの領域に，また K_2O-SiO_2 図上ではショショナイト－高カリウム系列上にプロットされる．Na_2O や Rb にも富んでいる．ガリウム量は斑れい岩を除き 18 ppm Ga 以上と多く，A タイプ的な傾向を持つ．足摺岬花崗岩類の最大の特徴は HFSE (high-field strength elements) に富むことにある．Zr は最大で 1,220 ppm 含まれ，Hf (<25.6 ppm), Nb (<202 ppm), Ta (<14 ppm), LREE (<1,002 ppm), HREE (<50.5 ppm), Y (<74 ppm), Th (<74.2 ppm) にも富んでいる．またフッ素 (<0.43 wt.% F) が多く含まれる．

これらの微量成分は多数の副成分鉱物に含まれるが，一般的な鉱物はジルコン，チタン鉄鉱，褐簾石，チタン石などである．ジルコンはもっとも普遍的にみられ，まれに肉眼で識別できることもある．ジルコニウムの最大含有量を持つ 58A142 試料中のジルコンは，2.4 wt.% 以下の HfO_2，1.0 wt.% 以下の Y_2O_3 を含む．58A142 試料のチタン鉄鉱は 4.3-5.7 wt.% MnO を含むが，その他の石英閃長岩のチタン鉄鉱は低い値 (1.7-1.8 wt.% MnO) を持つにすぎない．チタン鉄鉱中のニオブは 3.8 wt.% Nb_2O_5 以下であり，チタン鉄鉱の縁に濃集するので，マグマ期最末期に熱水から添加されたものと考えられる．褐簾石は他形結晶として見られ，磁鉄鉱系花崗岩類に特徴的なマンガンに乏しい特徴 (0.44 wt.% MnO) を持つ．また，褐簾石は軽希土類元素に富み，24.6-25.8 wt.% LREE の範囲で比較的一定であるが，トリウム (0.05-3.7 wt.% ThO_2) は変化に富む．

足摺岬岩体の斑れい岩は最も苦鉄質な岩相で 47.0 wt.% SiO_2，12.5 wt.% MgO であり，上部マントルにその起源をもつものと思われる．閃長岩類は 55-60 wt.% SiO_2 で低い Sr 初生値 (0.7035) を持つことから，大陸地殻下部の苦鉄質岩を出発物質としているが，マグマの発生量が小規模であった為に，結果的にアルカリや HFSE に富んだと考えられる．北部の黒雲母花崗岩はこのマグマが四万十層群の堆積岩類を深所で同化して生成したと考えられる．足摺岬岩体の石英閃長岩類と関連岩脈類は異常な Zr, REE, Y を含むので，関連する熱水性鉱床を発見することは，REE 含有鉱床探査上のために重要である．

Plate IA Southern coastal view toward the Cape Ashizuri where alkaline granitoids are well exposed along the coastal cliff.
Plate IB Gabbroic blocks mingled with alkaline granitoids at the Cape Ashizuri, the same photo as one of the postcard set "Granites in Japan" by the Geological Museum, GSJ.

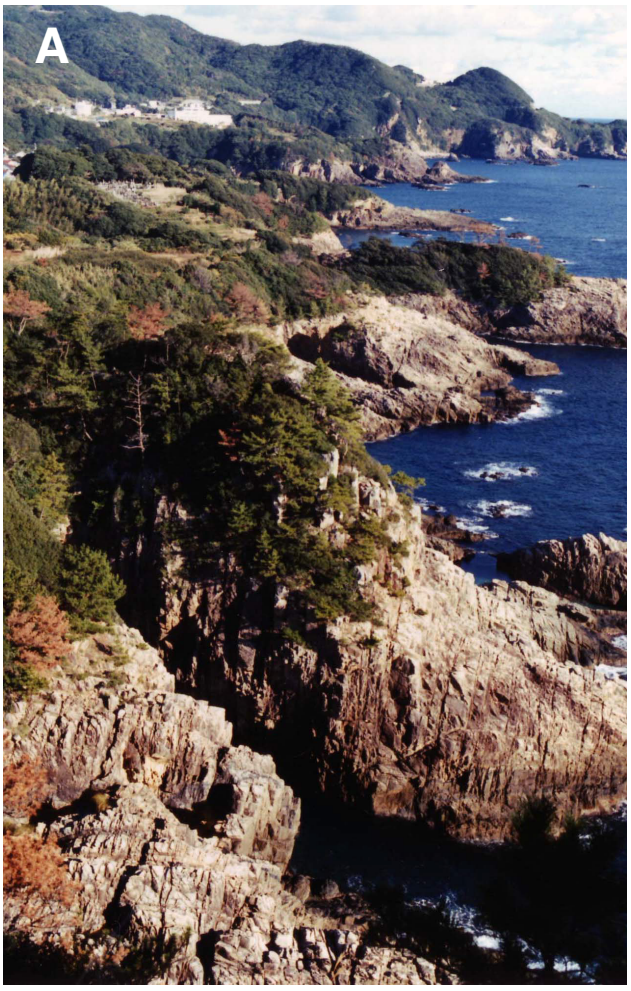

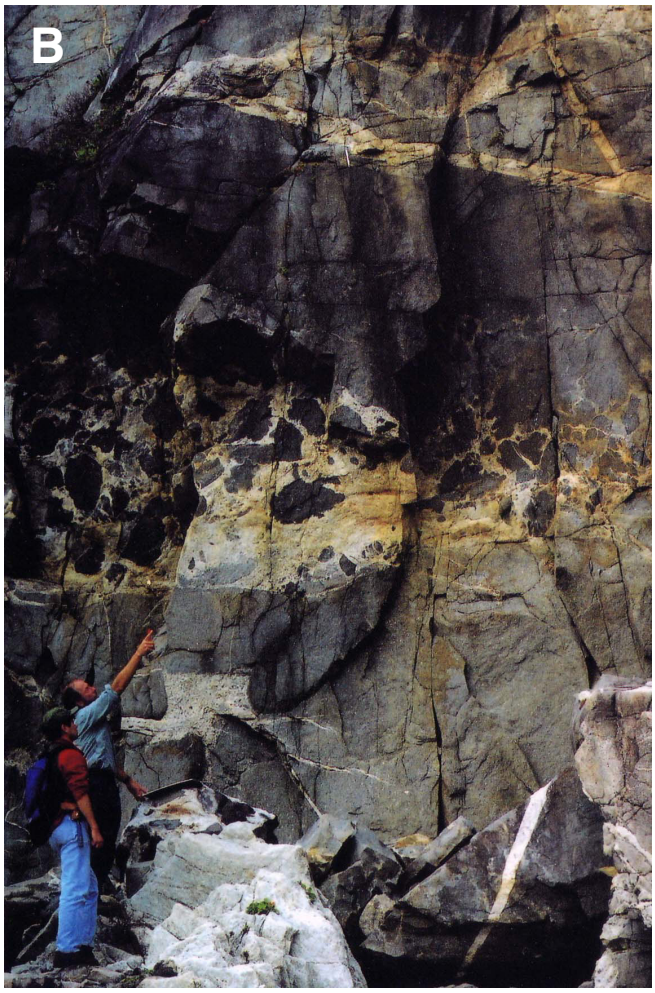

Plate II　Analyzed zircon (A-F) and allanite (G-I) crystals by EPMA. The white bar indicates 0.1 mm.

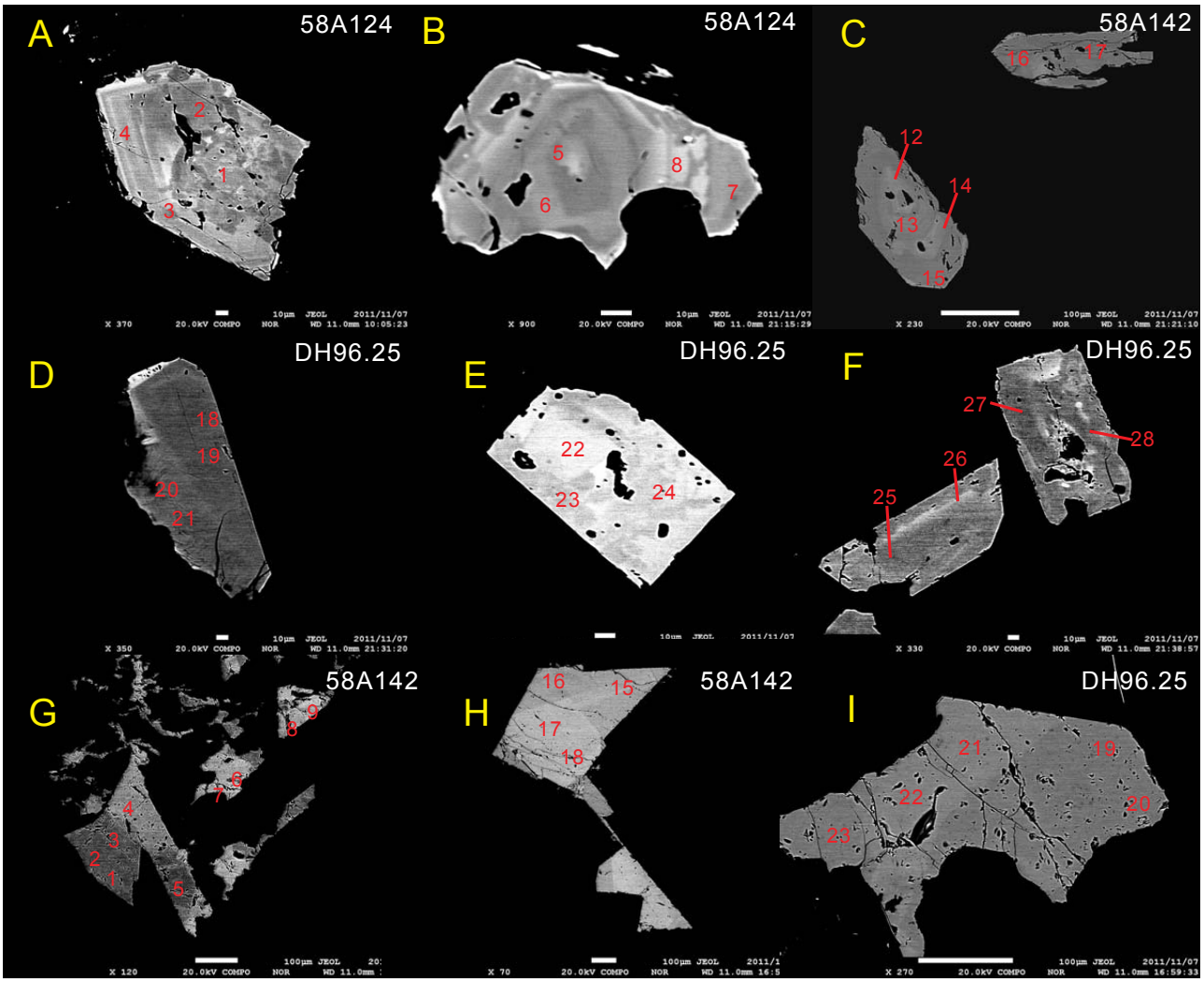

Plate III Analyzed titanite (A-C), fergusonite (D-F) and chevkinite (G-H) crystals by EPMA. The white bar indicates 0.1 mm.